Tectonophysics 597–598 (2013) 85–105

Contents lists available at SciVerse ScienceDirect

Tectonophysics

journal homepage: www.elsevier.com/locate/tecto

The Sparta Fault, Southern Greece: From segmentation and tectonic geomorphology to seismic hazard mapping and time dependent probabilities

Ioannis D. Papanikolaou [a,b,*], Gerald P. Roberts [b], Georgios Deligiannakis [a,c], Athina Sakellariou [a], Emmanuel Vassilakis [c]

[a] Mineralogy–Geology Laboratory, Department of Earth and Atmospheric Sciences, Agricultural University of Athens, Iera Odos 75, 118-55, Athens, Greece
[b] Department of Earth Sciences, Birkbeck College and University College London, WC 1E 6BT, London, UK
[c] Laboratory of Natural Hazards, Faculty of Geology and Geoenvironment, National and Kapodistrian University of Athens, Panepistimioupolis, 15784, Athens, Greece

ARTICLE INFO

Article history:
Received 6 August 2011
Received in revised form 3 August 2012
Accepted 27 August 2012
Available online 3 September 2012

Keywords:
Lakonia
Slip-rates
Active faults
Taygetos
Evrotas
Conditional probabilities

ABSTRACT

The Sparta Fault system is a major structure approximately 64 km long that bounds the eastern flank of the Taygetos Mountain front (2407 m) and shapes the present-day Sparta basin. It was activated in 464 B.C., devastating the city of Sparta. This fault is examined and described in terms of its geometry, segmentation, drainage pattern and post-glacial throw, emphasising how these parameters vary along strike. Qualitative analysis of long profile catchments shows a significant difference in longitudinal convexity between the central and both the south and north parts of the fault system, leading to the conclusion of varying uplift rate along strike. Catchments are sensitive in differential uplift as it is observed by the calculated differences of the steepness index k_{sn} between the outer ($k_{sn}<83$) and central parts ($121<k_{sn}<138$) of the Sparta Fault along strike the fault system. Based on fault throw-rates and the bedrock geology a seismic hazard map has been constructed that extracts a locality specific long-term earthquake recurrence record. Based on this map the town of Sparta would experience a destructive event similar to that in 464 B.C. approximately every 1792 ± 458 years. Since no other major earthquake M ~ 7.0 has been generated by this system since 464 B.C., a future event could be imminent. As a result, not only time-independent but also time-dependent probabilities, which incorporate the concept of the seismic cycle, have been calculated for the town of Sparta, showing a considerably higher time-dependent probability of $3.0 \pm 1.5\%$ over the next 30 years compared to the time-independent probability of 1.66%. Half of the hanging wall area of the Sparta Fault can experience intensities ≥IX, but belongs to the lowest category of seismic risk of the national seismic building code. On view of these relatively high calculated probabilities, a reassessment of the building code might be necessary.

1. Introduction

In 464 B.C. a major earthquake devastated the city of Sparta (~20,000 fatalities, ≥X MS intensity Galanopoulos, 1961; Papazachos and Papazachou, 1997), causing great social unrest. This event is regarded as the oldest well-defined event in the Hellenic historical record and is described by plethora of ancient authors such as Thucydides, Diodoros, Aelianos and Plutarch (e.g. Galanopoulos, 1961; Papazachos and Papazachou, 1997). This major event is clearly associated with the Sparta Fault (Armijo et al., 1991), which is located only a few km westwards from the city of Sparta and forms the only major seismic source that can generate such a strong earthquake.

Despite this strong event, the area of Sparta is characterised by low seismicity over the last 25 centuries since no other major event has occurred in the town of Sparta since 464 B.C. (Papanastassiou, 1999). Therefore, since sufficient time has elapsed for stress to gradually re-accumulate, a future event on the Sparta Fault could be imminent. This is also supported by cosmogenic isotope dating techniques applied on the Sparta bedrock scarp, showing that the central and southern part of this fault did rupture repeatedly (at least six times over the past 13 kyr), with time intervals ranging from 500 to 4500 yr (Benedetti et al., 2002).

This fault is studied based on its post-glacial scarp, the analysis of the drainage network and the major catchments that are influenced by footwall uplift. In addition, we provide a seismic hazard map based on the geological fault slip-rate data from the Sparta Fault and estimate how many times the town of Sparta has received enough energy to shake at intensities ≥IX since the last glaciation. Moreover, by combining the long-term earthquake recurrence record with the historical record and the paleoseismological data, we have extracted time-independent and time-dependent probabilities for large (characteristic) earthquakes. Time dependent probabilities incorporate the most basic physics of the earthquake cycle, are thus

* Corresponding author at: Mineralogy–Geology Laboratory, Department of Earth and Atmospheric Sciences, Agricultural University of Athens, Iera Odos 75, 118-55, Athens, Greece.
E-mail addresses: i.pap@aua.gr, i.papanikolaou@ucl.ac.uk (I.D. Papanikolaou).

0040-1951/$ – see front matter © 2012 Elsevier B.V. All rights reserved.
http://dx.doi.org/10.1016/j.tecto.2012.08.031

important considering the prolonged elapsed time since the last event on the Sparta Fault.

2. The Sparta Fault system

The Sparta Fault system (Figs. 1–3) bounds the eastern flank of the Taygetos Mt (2407 m) and shapes the western boundary of the Sparta–Evrotas basin (Fig. 2). This fault zone belongs to the arc parallel normal faults with a NNW–SSE to N–S trend from the Ionian to the Aegean Sea that create the alternation of neotectonic horsts (Methoni, Taygetos/Mani, Parnon) and grabens (Kalamata/Messiniakos Gulf, Sparta/Lakonicos Gulf) (Mariolakos and Papanikolaou, 1981; Lyon-Caen et al., 1988; Papanikolaou et al., 1988). The Taygetos Mt is a tectonic horst that is constantly uplifted and bounded by the Sparta and Kalamata Fault systems eastwards and westwards, respectively (Mariolakos and Papanikolaou, 1981). Both fault systems ruptured in historical times. The 1986 (Ms = 6.2) Kalamata earthquake ruptured one of the segments of the Kalamata Fault system producing surface ruptures over a few km and a maximum displacement of 20 cm (Lyon-Caen et al., 1988; Mariolakos et al., 1989).

The Sparta Fault trends NNW–SSE and has a length of 64 km. Its southern tip is located close to the Gerakari catchment approximately 3–4 km southwards from the Potamia village, whereas its northern tip towards the Alfios river, a couple of km westwards from the Kamaritsa village in the Megalopolis basin (Fig. 1). This active fault largely follows the Miocene detachment of East Taygetos Mt which

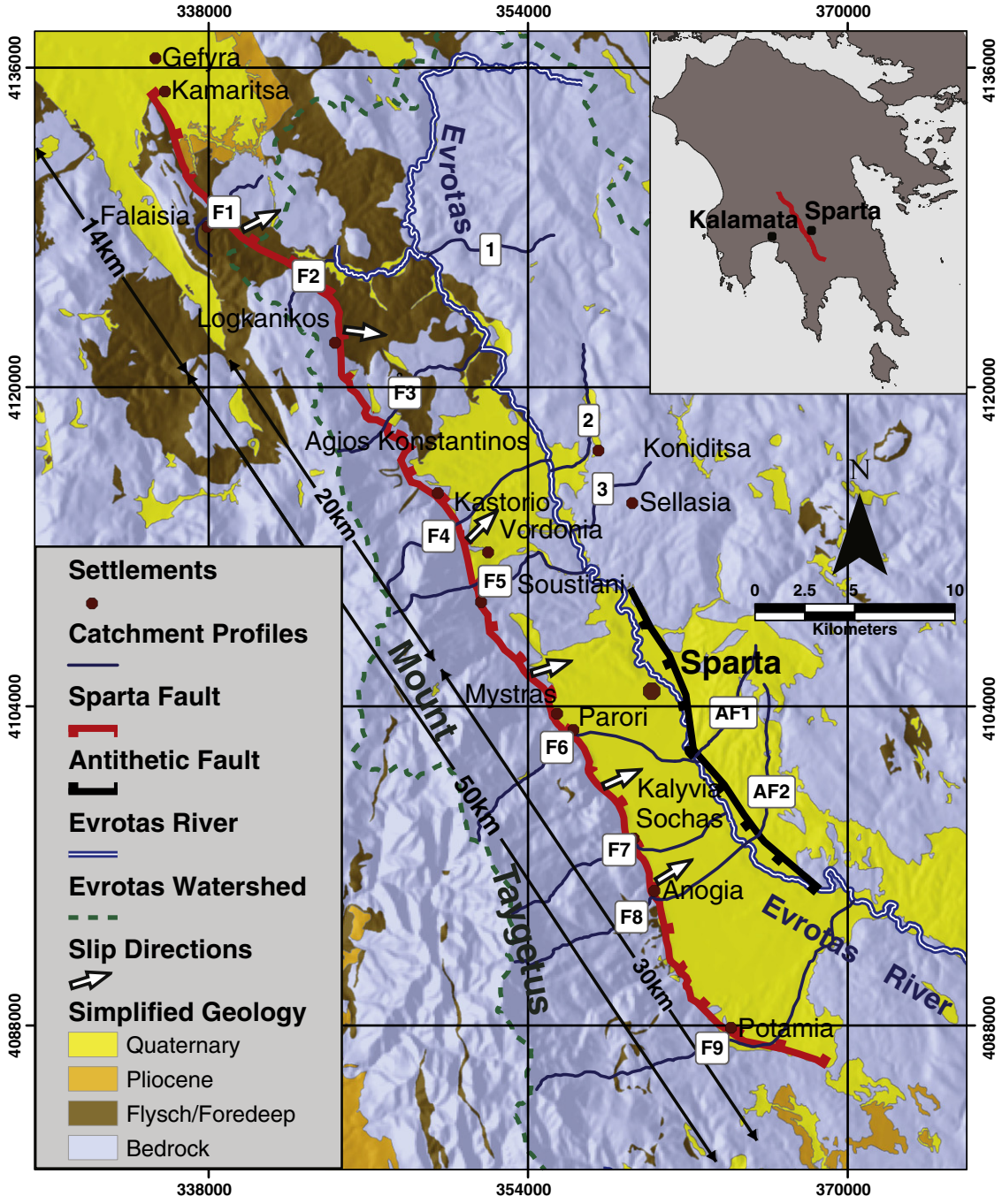

Fig. 1. Simplified geological map of the area of Sparta. Arrows represent fault slip directions. Catchments' profile numbers correspond to Fig. 6. Coordinates are in EGSA 87 which is the official Greek Coordinate System. It is metric, uses GRS 80 as a reference ellipsoid and it is a Transverse Mercator Projection which covers the whole country.

is also parallel to the main low angle extensional structure of the East Parnon Mt (Papanikolaou and Royden, 2007). However, the Sparta Fault can be divided in segments with different throws as this is revealed by the changes along strike of the Alpine units cropping out in the footwall as well as in the hanging wall (Fig. 2a). The nappe pile in Taygetos and Parnon comprises the Mani autochthon and the nappes of Arna, Tripolis and Pindos (Papanikolaou and Royden, 2007). Thus, the fault between Anogia and Mystras villages separates the Mani autochthon at the footwall and Plio-Quaternary sediments overlying the Arna metamorphics in the hanging wall. A similar

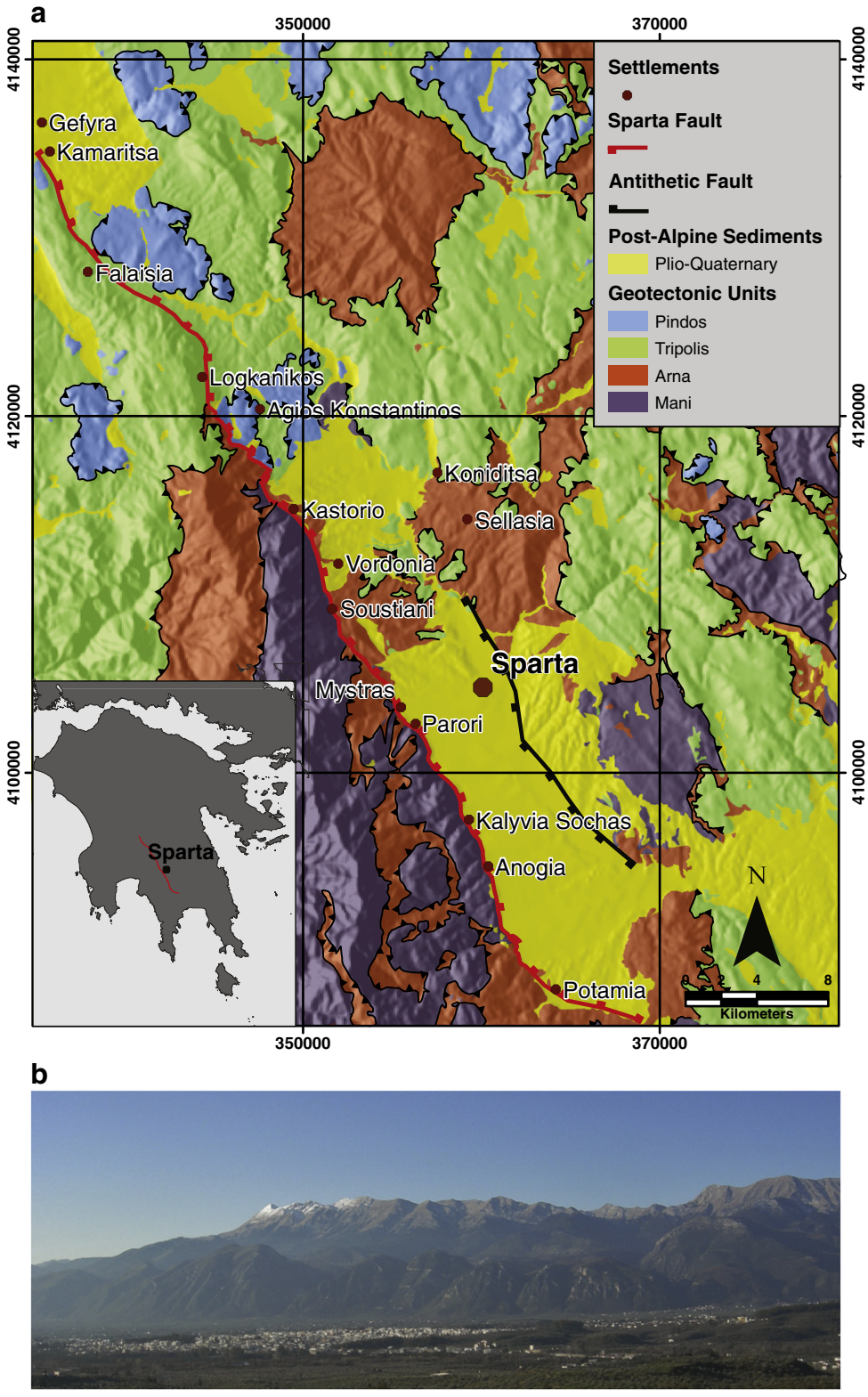

Fig. 2. a) Simplified geological map showing the geotectonic units outcropping the area. b) Distant view of the Sparta Fault. It uplifts the Taygetos Mt on its footwall and shapes the basin of Sparta towards its hanging wall. There are two ridges shown in the photo, a lower one in front bounded by the Sparta Fault, and a higher summit ridge behind; in between lies the relic of the easily erodible Arna unit, consisting of schists.

view is observed towards the central part of the fault between Vordonia and Kastori villages. However, towards the central part between Mystras and Vordonia villages as well as towards the southern tip, southwards Anogia village, the footwall is comprised of the Arna metamorphics and the hanging wall consists of the Plio-Quaternary sediments overlying the Arna metamorphics, implying a lower total

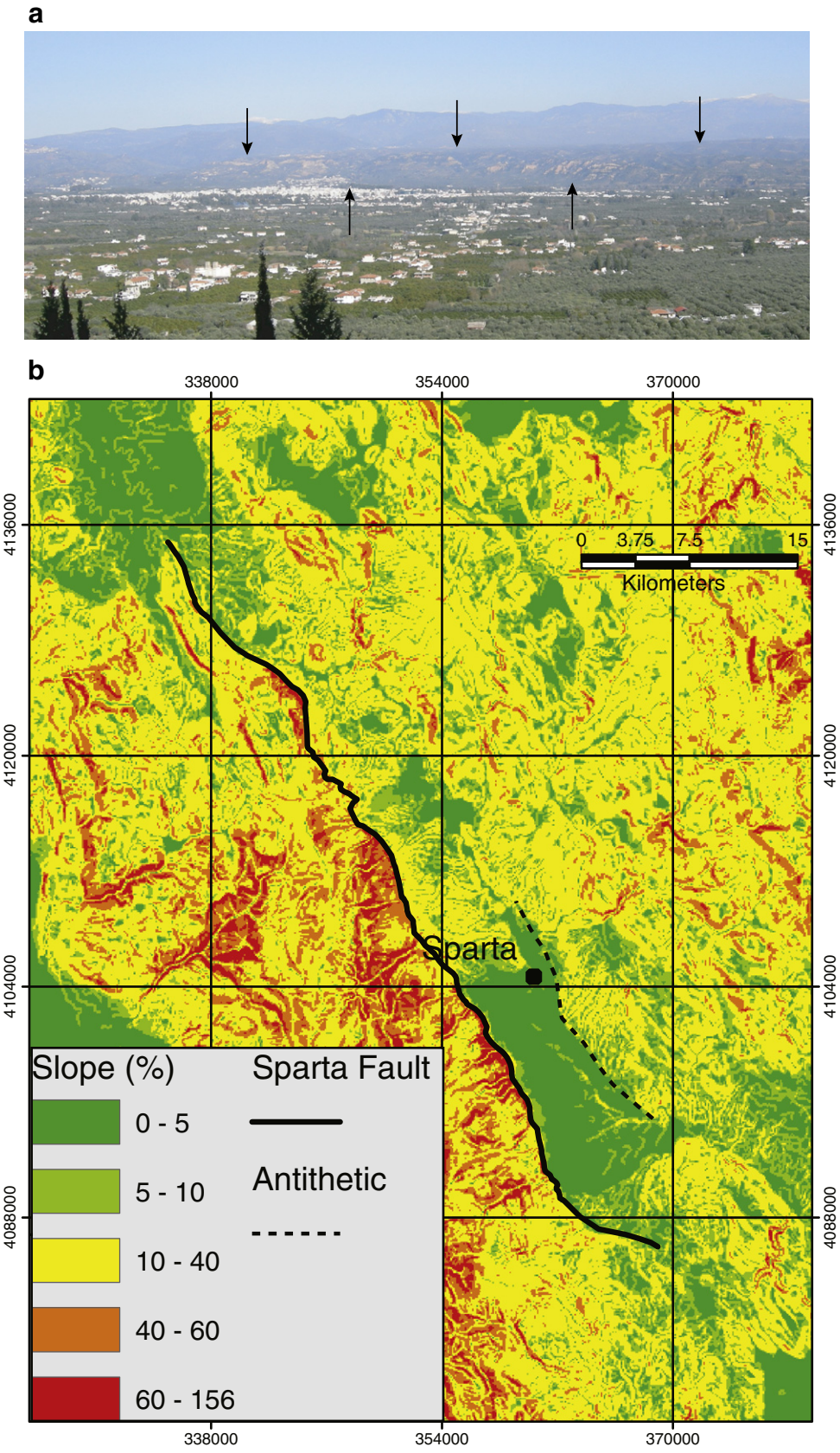

Fig. 3. a) View of the antithetic Sparta Fault from the west. It forms a topographic relief of a couple of hundred metres and defines the eastern boundary of the Sparta basin and the Evrotas river channel. b) Slope dip map of the study area where the linear traces of the main and antithetic Sparta Fault are clearly revealed.

throw. In addition, between Mystras and Vordonia the Quaternary sediments are thin or absent, so that the Arna unit outcrops in the hanging wall. Finally, towards the northern tip, northwards Logkanikos village, the footwall is composed of the Tripolis Mesozoic carbonates and the hanging wall the Tripolis Eocene flysch and in places the overlying Pindos nappe, implying a lower total throw (less than 1 km). Overall, this is a complex structure that has accommodated up to 5–6 km of throw. However, a significant part of this throw relates to the detachment activity in Upper Miocene–Lower Pliocene time, whereas its Quaternary throw varies from several hundred metres up to 2 km, forming a smaller portion of the total throw.

The immediate hanging wall of the Sparta Fault is characterised by major alluvial fans and steep triangular facets (e.g. Armijo et al., 1991; Pope et al., 2003), whereas in the immediate footwall highly incised catchments and wineglass canyons are the evidence of the high uplift rates (Fig. 2b). Moreover, particularly towards its central and southern part it has a fault zone up to 3 km wide in places with older fault planes existing towards the footwall, attesting to its long history of rupturing. It is clear following the boundary between Alpine rocks and Pleistocene sediments, as well as from the well exposed post-glacial scarp, that activity has shifted eastwards to a more basinward fault plane, following a progressive hanging wall directed migration within the fault zone (e.g. Stewart and Hancock, 1994). The post-glacial age of the scarp is confirmed by the ^{36}Cl cosmogenic isotope dating by Benedetti et al. (2002). The post-glacial scarp offset smooth hillsides that are typical of former periglacial processes, providing a regional marker of known age (Fig. 4). Even though no glaciers exist today, periglacial processes represent an important geomorphological agent on the highest peaks (Hughes et al., 2006). The Peloponnese and Crete display evidence of former glaciation and intense periglacial activity (Mastronuzzi et al., 1994; Hughes et al., 2006). In particular, Mastronuzzi et al. (1994) describe glacial landforms (e.g. cirques, morainic arcs and preserved unweathered moraines) towards the eastern flank of the Taygetos Mt on the footwall of the Sparta Fault, estimating a Wurmian (ELA) (mean equilibrium line altitude or snow line) lower than 2000 m. It is clear that periglacial activity extended down to much lower altitudes (Hughes et al., 2006). Similar post-glacial scarps have also been described southwards towards the island of Crete (Caputo et al., 2006). The Sparta Fault is made up of several en echelon segments of different lengths. However, two major faults are traced within this structure. The northern segment is about 14 km long and characterised by lower slip-rates. No post-glacial scarp was identified in the northern segment of the fault, implying that slip-rates are low and most probably less than <0.3 mm/yr (e.g. based on the comparison between trench sites and post-glacial scarps in the Apennines; Papanikolaou, 2003). On the other hand, the southern segment is 50 km long and leaves the most impressive imprint in the topography, showing signs of recent intense activity. The southern segment can be divided into two major sub-segments. In the recent past they were probably two individual structures that are now hard-linked (see justification in the Discussion section). Although local oblique or strike-slip motions occur near fault tips, as is common in extensional areas (Roberts, 1996; Roberts and Ganas, 2000), extension in the Sparta Basin based on fault slip data is predominantly ENE–WSW dip-slip (Fig. 1). Roberts and Ganas (2000) proposed two faults within this system based on the slip-directions which coincide with the two sub-segments we have divided in this study. This fault exhibits an impressive post-glacial scarp that can be traced for many km (Fig. 4). In particular, from the village of Anogia up to the area of Mystras, it is continuous and displays an 8–12 m high post-glacial scarp (Armijo et al., 1991; Papanastassiou, 1999; Benedetti et al., 2002).

The northern segment of the Sparta Fault that is characterised by lower activity and where no post-glacial scarp is revealed, displays a relatively low dip fault plane that ranges from 38° up to 52° (a mean of 43°), whereas the southern longer segment displays steeper fault planes dipping westwards from 38° up to 80° (a mean of 62°). The southern segment is characterised by an extensive post-glacial scarp of several metres. The maximum post-glacial throw of 8–12 m is displayed towards the centre of the segment from Anogia to Parori and gradually decreases towards the tips (Fig. 5). In Logkanikos village the post-glacial scarp is estimated at 5 m (Fig. 5c), the fault plane dips at 65° towards ENE (075°), whereas the striations are plunging at (63°) towards east (097°), thus converging towards the hanging wall centre. Two detailed topographic profiles were constructed perpendicular to the post-glacial fault scarp in Anogia, in localities that display the maximum and minimum observed throw, a few tens of metres distant from each other. These localities are undisturbed by erosion or deposition and the upper and lower slopes are adequately exposed. Striations are plunging towards NE (058°) and fault plane dips at 63° towards east (088°), thus

Fig. 4. Distant view of the post-glacial scarp of the Sparta Fault in the Kalyvia–Sochas locality. The post-glacial scarp offset smooth hillsides that are typical of former periglacial processes, providing a regional marker of known age (15 kyr ago ± 3 kyr).

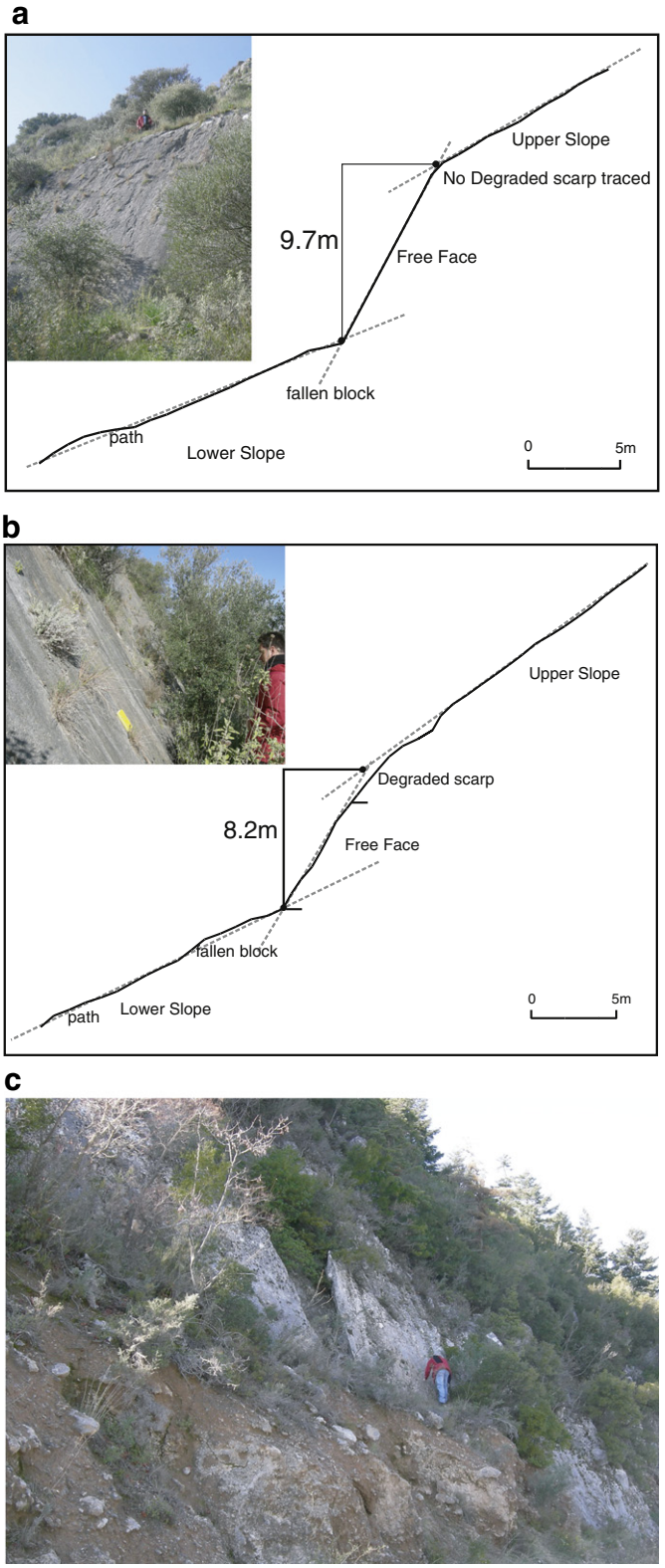

Fig. 5. a) Detailed topographic profile of the post-glacial scarp of the Sparta Fault near the village of Anogia, where the highest throw is observed. It is a 9.7 m high free face, where no imprint of a degraded scarp is traced (e.g. degraded scarp; the eroded lower-angle extension of the bedrock fault plane). b) Detailed topographic profile of the post-glacial scarp of the Sparta Fault near the village of Anogia, where the lowest throw is observed. This is an 8.2 m high scarp with approximately 6 m of free face and 2 m of degraded scarp. c) View of the 5–6 m high post-glacial scarp of the Sparta Fault near the Logkanikos village.

converging towards the hanging wall centre, implying that it is predominantly a normal fault. The profile with the maximum throw in Anogia, exhibit 9.7 m that comprises entirely the free face (Fig. 5a). No signs of the degraded scarp were traced, as is usually the case where it could represent 30 or even 40% of the scarp (Papanikolaou et al., 2005). The profile with the minimum throw exhibits 8.2 m (Fig. 5b). This variation of 1.5 m that represents the inherent surface throw variability is rather small and accounts for less than the usual 20% variability in such measurements (Papanikolaou et al., 2005; Papanikolaou and Roberts, 2007). The latter implies that surface ruptures maintained a relatively constant throw exhibiting more or less the same cumulative slip pattern from successive events over time.

It is also interesting to note that beyond the main Sparta Fault system there is also a significant antithetic structure approximately 5 km eastwards from the main fault (Fig. 3a). Both structures shape the present day Sparta basin forming linear features as this is also evident from the slope dip map (Fig. 3b). This map shows not only the dominant control that the main Sparta Fault exerts in the topography, but also the significant influence of the antithetic Sparta Fault. The Sparta–Evrotas basin is a neotectonic basin with post-alpine sediments. The easternmost boundary of the old neotectonic basin is now traced towards the Parnon Mountain front, it is fragmented, widely distributed and is characterised by low activity. The present-day active antithetic fault zone that bounds eastwards the Evrotas–Sparti basin appears towards the centre of the older neotectonic basin and is located approximately 10 km west from the Parnonas Mt. The antithetic structure is trending NNW–SSE has a length up to 18 km and dips westwards. It controls the topography of the area (Fig. 3a), forming a ~150 m throw based on the topographic variation and the thickness of the Plio-Pleistocene sediments (estimated a couple of hundred metres). This antithetic structure is active, linear, forming a topographic relief of a few hundred metres, defines the eastern boundary of the Sparta basin and bounds not only the Upper Pleistocene–Holocene sediments, but also controls the Evrotas flow. No clear estimate on the slip-rate can be made. Due to its short distance (~5 km) from the Sparta Fault, this antithetic structure most probably is linked at depth with the main Sparta Fault.

3. Tectonic geomorphology; catchments and tectonic uplift

The Evrotas river flows through the Sparta Basin, parallel to the Sparta Fault, trending NNW–SSE, while the secondary branches of this fluvial system consist of transient rivers which flow perpendicular to the main structure. The asymmetry of the drainage basin and this combination of fault parallel and fault perpendicular flow, indicates a strong tectonic control to the drainage pattern and is characteristic of active normal faulting settings (e.g. Gawthorpe and Hurst, 1993; Eliet and Gawthorpe, 1995). Landscape response to various uplift rates has been widely studied in terms of mountain fronts and catchments profiles (Kirby and Whipple, 2001; Silva et al., 2003; Cowie et al., 2008; Turowski et al., 2009). In this section, we examine the drainage network and the major catchments that are influenced by footwall uplift. In order to examine the transience of the streams across the Sparta Fault, cross sections perpendicular to the river flow in the headwaters and within the downstream convex reach were analysed (Figs. 6 and 7). This analysis may offer information regarding differential uplift rates (e.g. Kirby and Whipple, 2001).

3.1. Methodology

Fluvial long profiles of the transient rivers crossing different segments of the Sparta Fault were constructed in order to examine their longitudinal convexity and its variation along strike. Such profiles were also compared to the longitudinal profiles of neighbouring catchments that are not influenced by any fault. Geological data of the area, in conjunction with a 25 m resolution digital elevation model (DEM) were digitised, transformed into raster data and imported in ArcGIS Version

9.3. Slope map and catchments profiles were extracted by DEM surface analysis elaboration, while interpretation and calculation of the k_{sn} of catchment profiles was rendered by the combination of ArcGIS Profiler Toolbar and codes in Matlab version 7.10.0.499 (Whipple et al., 2007).

We also calculated the normalised steepness indices, k_{sn}, using a reference value of concavity index (θ) in the power low function:

$$S = ks \cdot A^{-(\theta)}$$

where A represents the drainage area, S is the local channel gradient or river slope and ks and θ are referred to as steepness and concavity indices, respectively. The use of the normalised steepness index was proposed by Duval et al. (2004), as more significant in case of approaching the relative, rather than absolute, spatial variations in channel characteristics. Several authors have demonstrated that high k_{sn} values are related to higher uplift rates (e.g. Wobus et al., 2006; Whittaker et al., 2008). Kirby and Whipple (2003) demonstrated that tectonically unperturbed "equilibrium" fluvial long profiles are typically smooth and concave-up. However, upland rivers are also sensitive to along-stream variations in differential uplift (potentially leading to changes in the profile concavity or steepness index) and also to changes in uplift rate through time. Whittaker et al. (2008) showed that rivers with drainage areas greater than 10 km^2 and crossing faults that have undergone an increase in throw rate within the last 1 Myr, have significant long-profile convexities. They also established that this relationship holds for throw rate variation along strike the same fault segment, as

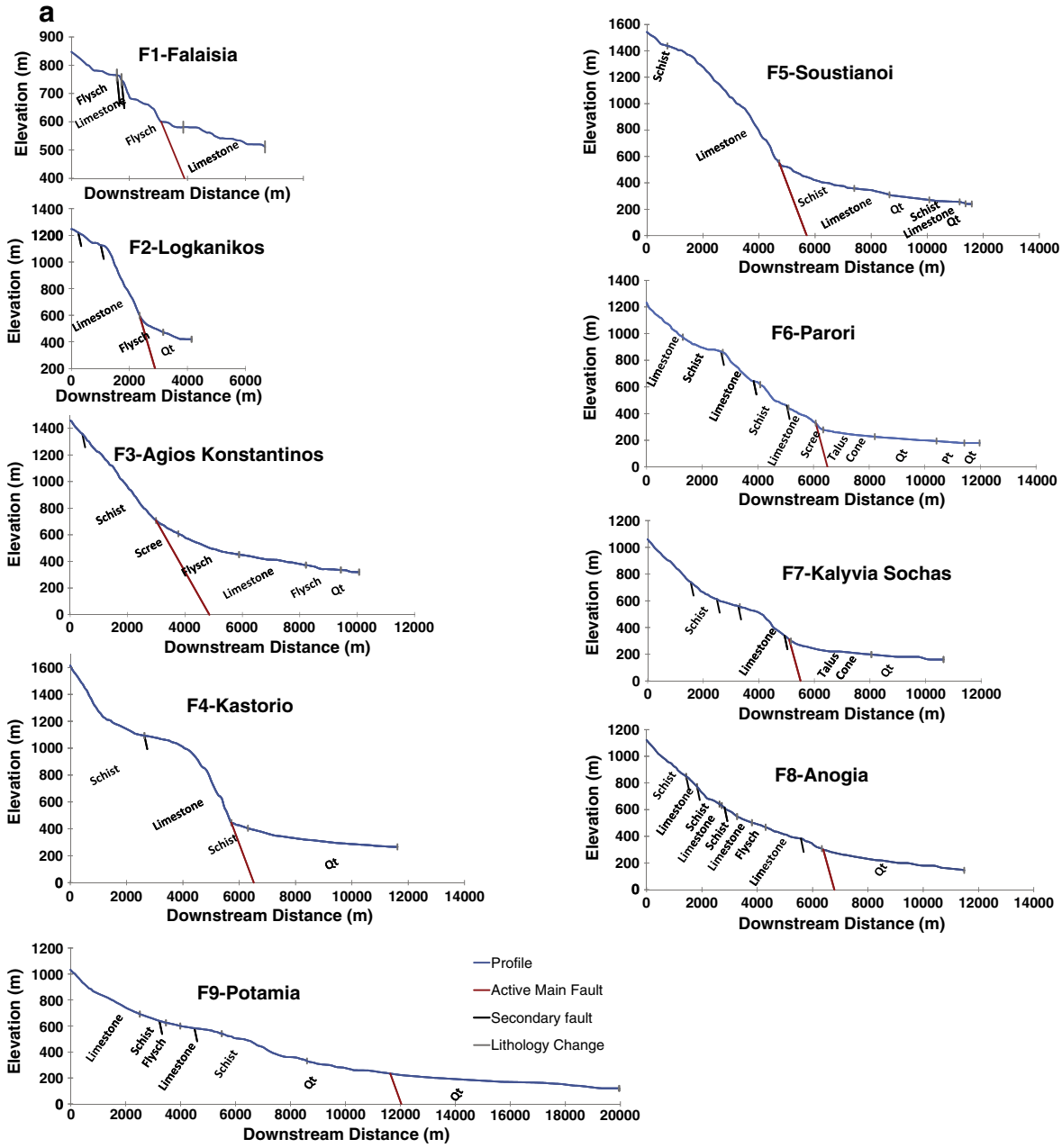

Fig. 6. a) Long profiles of rivers crossing perpendicular the Sparta Fault near the Potamia, Anogia, Kalyvia–Sochas, Parori, Soystianoi, Kastorio, Ag. Konstantinos, Logkanikos and Falaisia villages, respectively. Locality names are shown in Fig. 1. b) Long profiles of rivers crossing the antithetic Sparta Fault as well as rivers that cross no active fault near the Sellasia, Koniditsa and Kollinaitiko villages. Locality names are shown in Fig. 1.

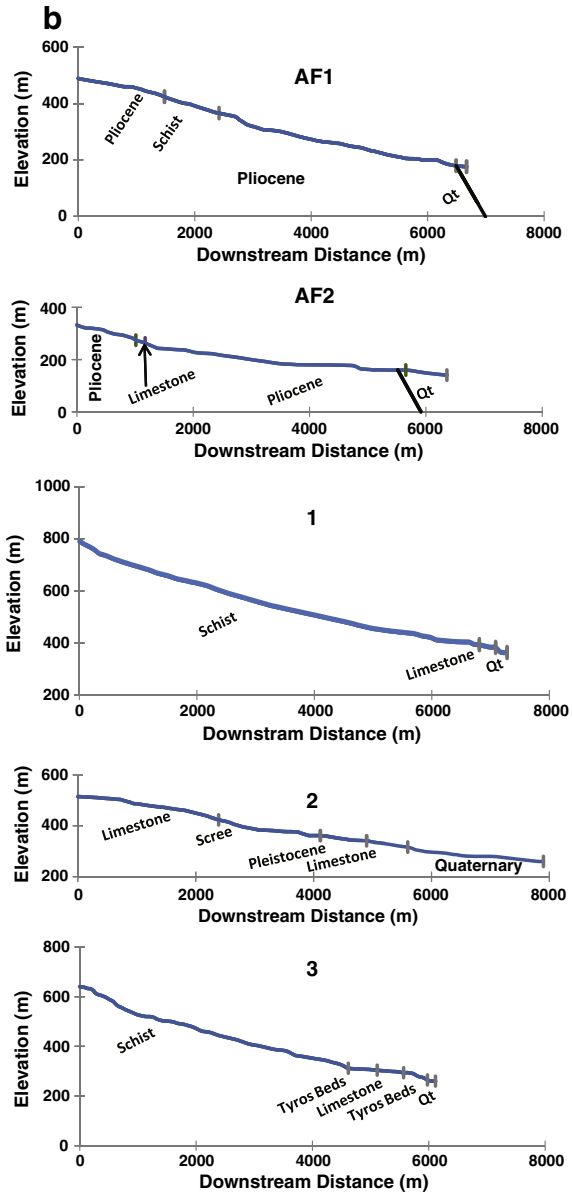

Fig. 6 (*continued*).

well as between faults. Moreover, Boulton and Whittaker (2009) suggested that rivers crossing active faults are undergoing a transient response to ongoing tectonic uplift and this interpretation is supported by typical signals of transience such as gorge formation and hill slope rejuvenation within the convex reaches.

While river long profile convexities can lead to the observation of the ongoing tectonic uplift, differential erosion of geological formations may also cause the same pattern. Thus, in order to exclude the latter phenomena and emphasise the tectonic uplift, the rivers to be examined must fulfil some restrictions. Whittaker et al. (2008) suggest that the selected rivers should discharge a drainage basin larger than 10 km^2 above the fault and the upstream length should be at least 5 km for extracting meaningful results. These restrictions are applicable in the south and central parts of Sparta Fault, as well as in the antithetic structure and areas of high topography, but with no active faulting. However, in the northern part of the Sparta Fault catchments are not long enough to fulfil these criteria, due to the proximity of the watershed of Evrotas Basin to the NW part of the fault.

3.2. Results

In total 9 profiles of transient rivers crossing different parts of the Sparta Fault were constructed (Fig. 6a). All these 9 catchments have an approximately E–W trending flow direction, due to headward erosion, draining the footwall of the Taygetos Mt across the fault into the hanging wall and merge with the N–S fault parallel flow direction of the Evrotas river, due to hanging wall subsidence. In addition, such profiles were constructed in 2 catchments crossing the antithetic Sparta Fault structure and were also compared to the longitudinal profiles of 3 neighbouring catchments crossing high topography, but no apparent faults (Fig. 6b).

Qualitative analysis of long profiles showed a significant difference in longitudinal convexity between the central and both the south and north parts of the fault, leading to the conclusion of varying uplift rate along strike (Fig. 7). A minor convex reach of 205 m in Potamia catchment long profile (southeast part of the Sparta Fault) can be clearly observed although it seems to have propagated upstream in relation to the fault. This could happen as the channel successively adjusts to the imposed uplift field (Whipple and Tucker, 2002). On the other hand, Anogia river's flow with significant deviations downstream and through a rapid variation of different geologic formations upstream creates a long profile convexity that appears in a smaller scale (101 m) than the other profiles. The northernmost of the two above catchments, Kalyvia–Sochas catchment long profile revealed a convex reach of 246 m, which is in contact with the Sparta Fault, in contrast to Potamia catchment's convex reach that is located 3 km away from the present day fault trace in the footwall. The Parori and Kalyvia–Sochas catchments are the localities where extensive alluvial fans outcrop (Pope et al., 2003).

Parori catchment long profile convex reach appears to consist of three separate knickzones that are possibly related to lithological variations, but could be interpreted as cumulative convexity with a height of 536 m. Located in the central part of the Sparta Fault, catchments near Soustianoi and Kastori villages have convex reaches whose downstream ends are in contact with the fault, outreaching 876 m and 590 m, respectively.

In the northern part of the Sparta Fault, the Agios Konstantinos catchment seems to have a concave-up channel profile, possibly indicating a constant and low slip rate, since it is located towards the northern tip of the fault. The lack of profile convexity of Agios Konstantinos can also be attributed to the lithology factor since it flows through the higher erodible schists rather than the limestones (Fig. 6a). Logkanikos and Falaisia catchment long profiles have significant convexities. However, as previously stated, their drainage basins above the fault are too small and the upstream lengths are too short to extract meaningful results.

On the other hand, catchments crossing the antithetic structure as well as neighbouring areas where no active faults are traced display similar characteristics, such as typical concave up profiles with small exceptions related only to differential erosion (Fig. 6b). Such examples form a minor convexity that does not exceed 100 m on a catchment near Koniditsa (Fig. 6b, profile 2), due to profile long alterations in lithology and a 30 m high knickzone appearing in the last few hundred metres downstream Kolliniatiko river, related to the same lithological conditions that mark the transition from limestone to flysch or alluvial deposits. In both cases the convexity coincides with the transition from limestone to flysch or alluvial deposits, indicating the strong control of the lithological factor.

Finally, the normalised steepness index, k_{sn}, using a reference concavity of 0.45, was calculated for six catchments crossing all Sparta Fault parts, as well as for the two catchments crossing the antithetic structure and two catchments that cross no fault. The k_{sn} values for the catchments closer to the tips of the Sparta Fault (F3-Agios Konstantinos and F9-Potamia) were 90 and 82.7, respectively, while in the central part the steepness rates are higher and vary from 121

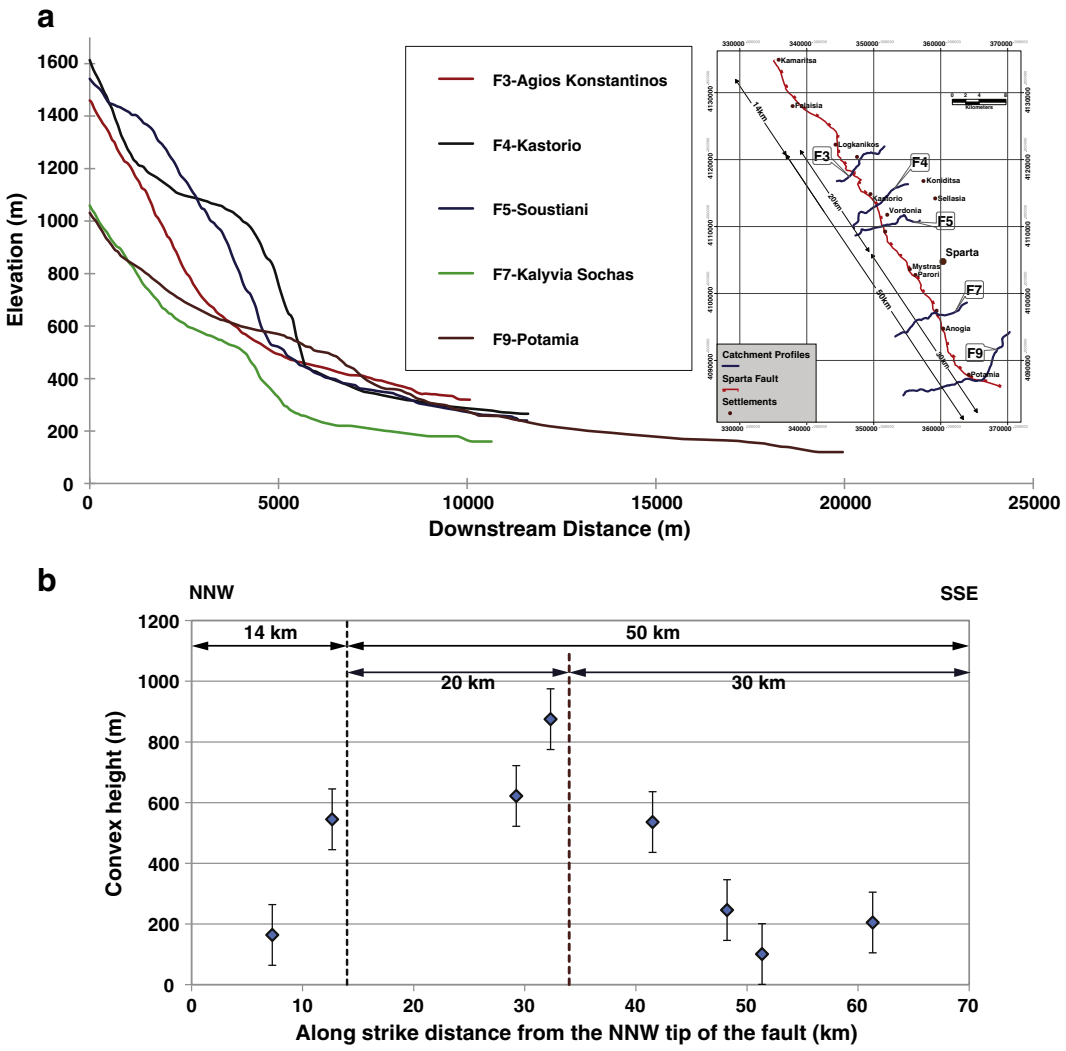

Fig. 7. a) Comparison of the catchments' profiles along strike the Sparta Fault. These profiles are sensitive to along-stream variations in differential uplift as observed from changes in their profile concavity or steepness index. Compare the differences between the Agios Konstantinos (northern part) and Potamia (southern part) with Soustianoi, Kastorio and Kalyvia–Sochas (central part) catchments' profiles. b) Diagram showing the convex height variability of the catchments along strike the fault system, with higher values towards its centre that diminish towards its tips. Error bar represents the 100 m convex height that can be attributed to differential erosion. There are 8 data points due to the lack of profile convexity of Agios Konstantinos that is attributed to the lithology factor since its entire footwall consists of the higher erodible schists rather than the limestones.

to 138 ($121 < k_{sn} < 138$). On the other hand, k_{sn} values for the catchments AF1 and AF2, crossing the antithetic structure, were 26.2 and 27.9, respectively, while the same normalised steepness index in catchments 2-Koniditsa and 3-Sellasia were 48 and 31.7, respectively. It is interesting to note that the profiles where no active fault is crossed exhibit higher values of k_{sn}, than the profiles that cross the antithetic Sparta Fault. This is a lithological effect since the catchments that cross the antithetic fault erode Quaternary sediments, whereas the catchments that cross no fault, flow through the alpine bedrock, which is more resistant to erosion.

4. Seismic hazard map from geological fault slip-rate data

Seismic hazard assessment tends to follow fault specific approaches where seismic sources are geologically constrained active faults (WGCEP, 1990, 1999, 2002; Ganas and Papoulia, 2000; Roberts et al., 2004; Papanikolaou and Papanikolaou, 2007; Pace et al., 2010) in order to address problems relating to the incompleteness of the historical records, obtain higher spatial resolution and realistic source locality distances, since seismic sources are accurately located. Thus, fault specific approaches are becoming very important for the seismic hazard assessment, by providing quantitative assessments through measurement of geologically recorded slip on active faults, providing a more reliable estimate of hazard than the historical earthquake record (e.g. Yeats and Prentice, 1996; Papoulia et al., 2001; Michetti et al., 2005). Based on slip-rate data and the fault geometry, we can construct seismic hazard maps purely from geological data (Papanikolaou, 2003; Roberts et al., 2004).

4.1. Data

Throw rates are extracted from the Sparta post-glacial fault scarp, using as a reference the last major glacial retreat phase that initiated 18,000 years ago (Giraudi, 1995; Allen et al., 1999). Also, ^{36}Cl exposure dating of a fault plane associated with a scarp revealed that the scarps are indeed post-glacial (Benedetti et al., 2002). Due to the uncertainty on the exact age we have used as post-glacial age an estimate of 15 kyr ± 3 kyr, whereas 18 kyr is the initiation of the last glacial retreat (Allen et al., 1999) that dominates the present geomorphology of the region and 12 kyr is the youngest reported age in the literature since

some small magnitude glacial re-advances followed by retreat phases have been recorded between 12 kyr ago and predominantly between 14 and 18 kyr ago (e.g. Giraudi and Frezzotti, 1997). The 1:50,000 geological maps (IGME Sheets Tataris et al., 1970; Psonis and Latsoudas, 1983; Psonis, 1986; Dimadis and Taktikos, 1989; Psonis, 1990; Papadopoulos, 1997; Zindros and Exindavelonis, 2002) were used for the generation of the digital geological layer (Fig. 1) and three types of bedrock geology have been differentiated that are associated with different shaking intensities during an earthquake: (a) Mesozoic/Tertiary limestone bedrock; (b) Tertiary Flysch and extensional basin-filling deposits; and (c) Quaternary sediments.

4.2. Methodology

This methodology was developed and is explained in detail in Papanikolaou (2003) and Roberts et al. (2004). Herein, it has been modified to fit the properties of the Sparta characteristic event that dominates the seismic moment release and has been recorded by the geological fault slip data. According to the cosmogenic isotope studies that are also confirmed by the 464 B.C. historical event, the Sparta Fault produces systematically maximum surface displacements of about 2 m that correspond to M 6.9–7.0 events. Such magnitude corresponds to approximately 30 km long ruptures. These ruptures float along the 64 km long fault, following the along strike variation of the fault slip-rate. The input data that governs the earthquake recurrence are fault throw-rates.

In particular, fault throw-rates are firstly converted into earthquake frequencies, assuming that each fault ruptures in "floating" earthquakes (e.g. WGCEP, 2002), which are distributed around a mean magnitude of fixed size. Then, this information is turned into a hazard map (see Papanikolaou, 2003; Roberts et al., 2004) after using: i) empirical relationships between coseismic slip values, rupture lengths and earthquake magnitudes, ii) empirical relationships between earthquake magnitudes and intensity distributions, and iii) attenuation/amplification functions for seismic shaking on bedrock compared to flysch and basin-filling sediments. The final product is a high spatial resolution seismic hazard map showing how many times each location has been shaken at a certain intensity value (e.g. intensity IX) over a fixed time period (e.g. since the last glaciation), which can be easily transformed into a map of recurrence intervals (Fig. 8).

Considering both the surface ruptures of the 464 B.C. historical event and the cosmogenic isotope dating where the mean displacement was 1.7 m in Anogia and 2.1 m in Parori, it is clear that the Sparta Fault ruptures in major earthquakes of approximately M = 7.0 (Benedetti et al., 2002). Moreover, the Parori that exhibits higher mean displacement is closer to the centre of the fault. Two of the seismic events (4.5 kyr ago and 5.9 kyr ago) were recorded in both sampling localities. Cosmogenic isotope dating showed that two events recorded in Parori were not recorded in Anogia and vice versa. Both localities are 10 km apart, confirming that different parts of the fault system were ruptured. Herein, it has to be acknowledged that some events towards the northern part of the fault may have not been traced in both cosmogenic site sampling localities, if surface ruptures did not reach or were of low displacement (less than 20 cm). Papanastassiou et al. (2005) support that the Sparta Fault ruptures approximately every 2000 years providing a M ~ 7.0 event that ruptures more than 22 km and based on some sedimentation rate variations supported that it might also produce moderate earthquakes M ~ 6.0, that may rupture a small part of the fault, but without substantial surface ruptures and displacements.

Therefore, following the above it is assumed that all surface slip is the result of floating earthquakes of magnitude M ~ 7.0, which are known to produce about 2 m of maximum slip with rupture lengths of about 30 km (e.g. regression from magnitude to SRL, Wells and Coppersmith, 1994; Pavlides and Caputo, 2004). Assuming a triangular throw profile for the fault (Cowie and Shipton, 1998) and earthquake surface ruptures, and that the maximum throw is observed at the centre of the fault (Fig. 8a), the number of surface faulting earthquakes of fixed size (M = 7.0), that the fault has experienced in a certain time period can be calculated (Fig. 8b). Therefore, since our time marker is the last glaciation then the bigger triangle simply represents the post-glacial cumulative seismic moment summation. Based on the inputs for the Sparta Fault approximately 13 M = 7.0 earthquakes have been extracted since the last glaciation. After calculating how many M ~ 7.0 earthquakes the fault has experienced during the past 15 kyr ± 3 kyr, modelled earthquakes are distributed according to the fault throw variation along strike of the fault trace. Taking into account the 3D normal fault geometry (e.g. Roberts et al.,

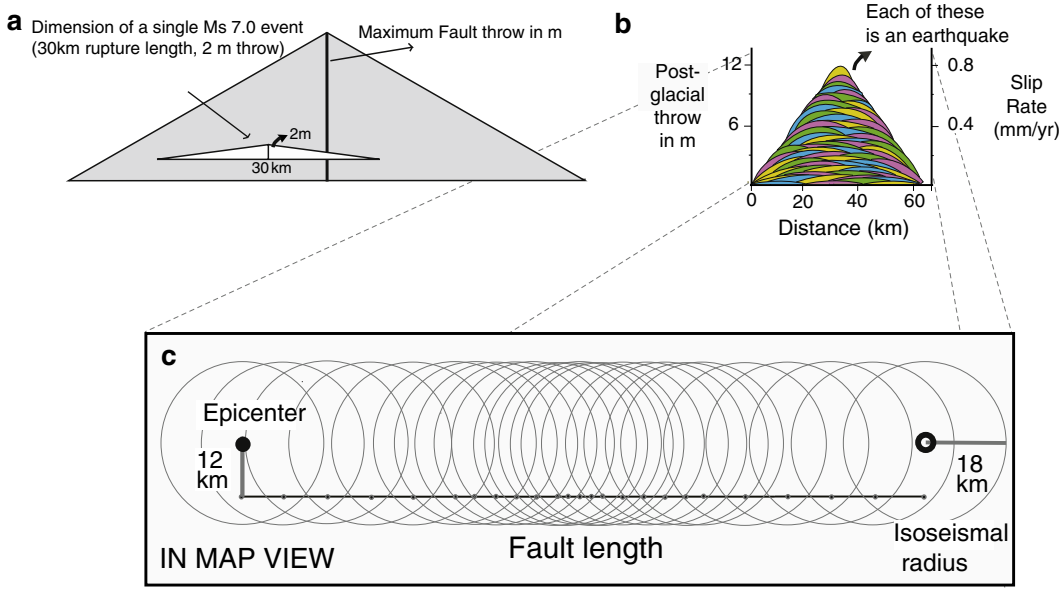

Fig. 8. Schematic representation for the construction of the hazard map, illustrating the concept of the methodology. a) Assuming that there is a triangular throw profile for the faults and ruptures and that the maximum throw is observed at the centre of the fault the number of surface faulting earthquakes of Ms = 7.0 can be calculated. b) Throw in this profile represent the slip that the fault has accumulated during the post-glacial period (since 15 kyr ago ± 3 kyr). c) Epicentres are plotted 12 km away from the fault in the hanging wall and circles with 18 km radius of intensity IX (representing "isoseismals") are added.

2004), hypothetical epicentres are plotted 12 km away from the fault in the hanging wall, assuming a 45° dipping fault and hypocentres at 12 km (Fig. 8c). These are realistic values because large seismogenic normal faults have dips in the range 30°–60° (Jackson and White, 1989) and large earthquake ruptures tend to nucleate close to the base of the seismogenic layer at 10–15 km depth (e.g. Sibson, 1984).

These isoseismals are then attenuated/amplified by the bedrock geology, altering their shapes, producing mostly elliptical shapes that result from the fact that the Quaternary basins are generally elongated in the direction of fault strike. Quaternary sediments are less dense and rigid compared to basement rocks so that their physical restraints on ground accelerations are limited and ground motions are enhanced in both amplitude and duration, resulting in higher damages and consequently to higher intensity values (e.g. Bolt, 1999). Finally, a simple model of three different shaking intensity levels was used, each one corresponding to different bedrock types (one for the bedrock, one for the flysch/foredeep deposits and another one for the Quaternary sediments). This classification of the geologic units into three major groups was chosen to correspond to the site conditions in terms of ground motion attenuation equations that are divided into hard rock (bedrock), soft rock (flysch and foredeep) and alluvium (Petersen et al., 1997; Park and Elrick, 1998). Several datasets that link surface geology and shaking intensity values suggest that there is approximately one degree of intensity difference between Mesozoic–Neogene limestones and pre-Quaternary sediments (such as flysch deposits or foredeep sediments) and another degree of intensity difference between pre-Quaternary and Quaternary sediments near the epicentral area (Medvedev, 1965; Evernden and Thomson, 1985; Degg, 1992).

4.3. Magnitude–intensity empirical relationships

For the Greek territory, magnitude–intensity laws and attenuation relationships are extracted from statistical elaboration of historical and instrumental data. However, there are significant differences between

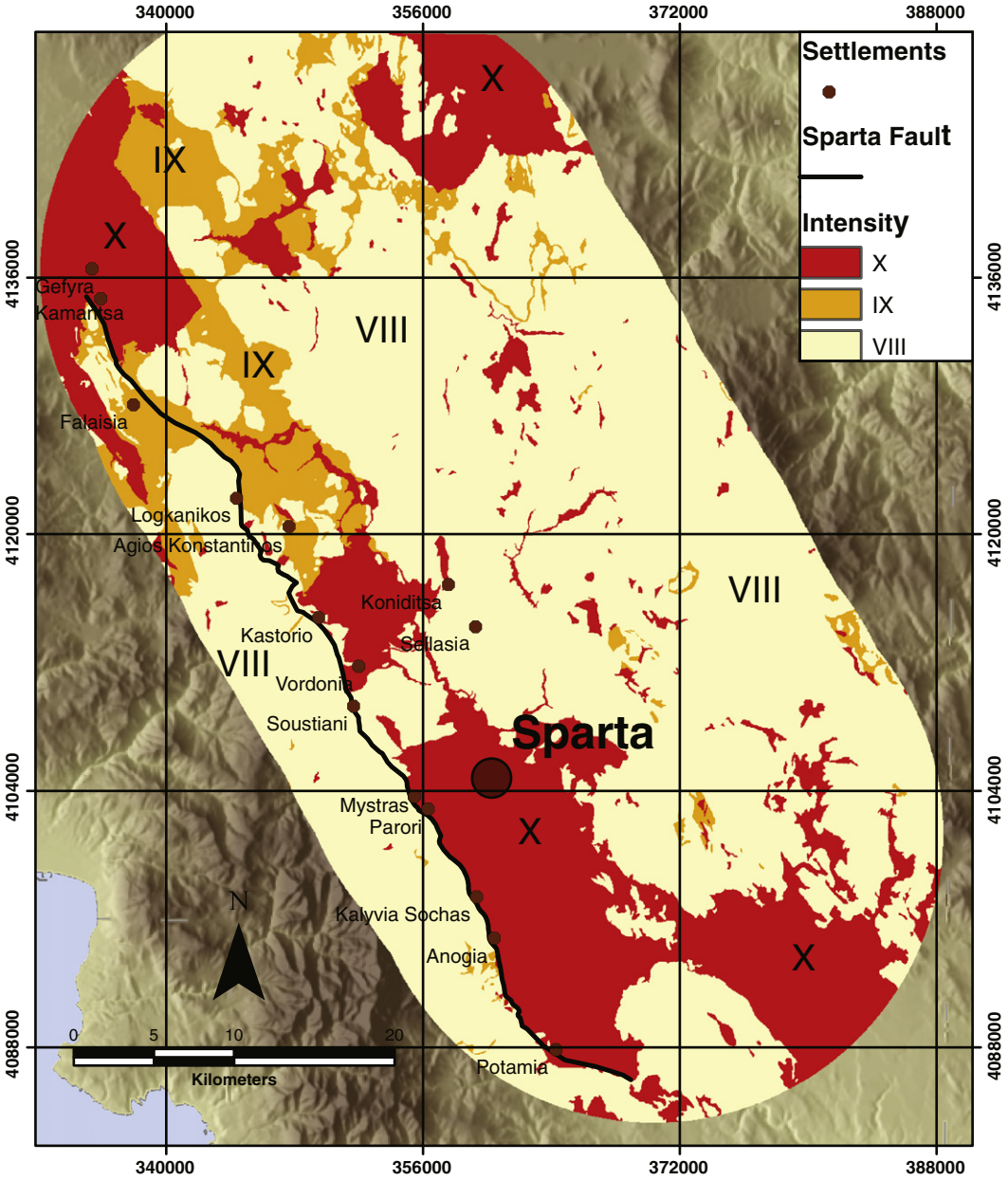

Fig. 9. Seismic hazard map for the Sparta Basin showing the maximum expected intensities that could occur in an infinitely long time period. The maximum intensity locations are defined by the proximity to the active faults and the bedrock geology.

published data regarding the relationship between magnitude, epicentral intensity and its attenuation with distance (Papaioannou, 1984; Theodoulidis, 1991; Papazachos and Papaioannou, 1997). More importantly, for an M = 7.0 earthquake, that a structure similar to the Sparta Fault is able to generate (Benedetti et al., 2002), only Theodoulidis's (1991) equations result in an epicentral intensity X, as has been clearly demonstrated by the Sparta 464 B.C. macroseismic field (Papazachos and Papaioannou, 1997). Theodoulidis (1991) proposes that a shallow earthquake with epicentral intensity X has a mean radius of 6–7 km for the X isoseismal and a mean radius of 16–18 km, for the isoseismal IX. Papaioannou (1984), and Papazachos and Papaioannou (1997) for a M = 7.0 earthquake estimate that intensity IX will cover an 8 km and 9 km radius from the epicentre intensity, respectively. Despite the differences, Theodoulidis' (1991) outcomes are also consistent with other worldwide intensity attenuation relationships in similar extensional tectonic settings such as central Apennines (Grandori et al., 1991) and south Korea (Lee and Kim, 2002) and are considered as more representative for the Sparta case study.

4.4. Results

4.4.1. Maximum expected shaking intensities

Fig. 9 shows which locations are expected to experience high or low intensities, but without specifying the possibility or probability of the assessment. The maximum intensity locations are defined by the proximity to the active fault and the bedrock geology. This map is useful because it can delineate areas that could experience severe shaking, from other areas which are situated further away from active faults and/or founded on bedrock, implying that they should experience less damage. Changing the dip of the fault or the seismogenic depth would slightly change the isoseismals even though the site's distance to the fault surface trace has not changed. However, the

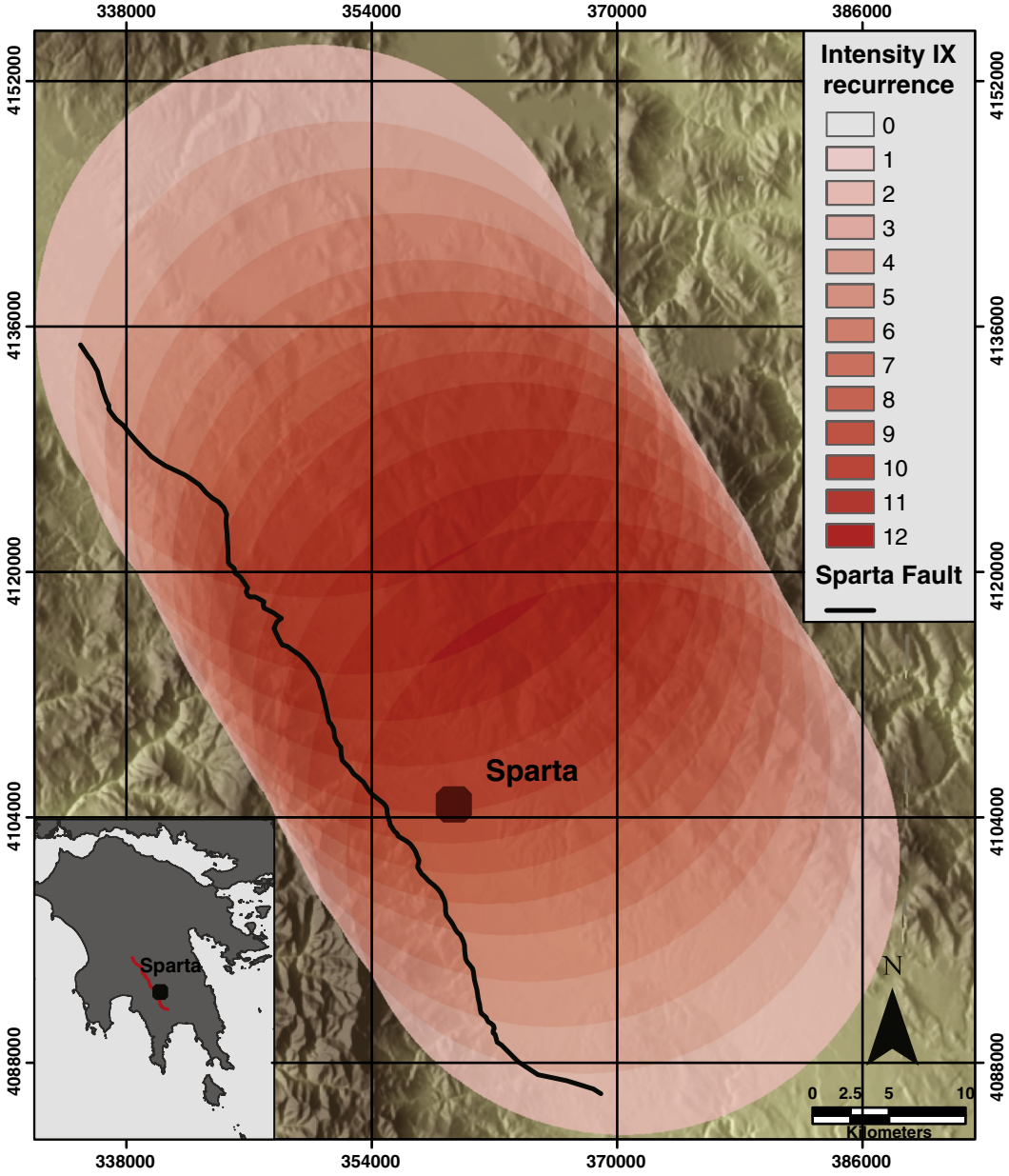

Fig. 10. Seismic hazard map for the Sparta Basin, showing how many times a locality receives enough energy to shake at intensities IX in 15 ± 3 kyr, assuming homogenous bedrock geology, a circular pattern of energy release and an 18 km radius of isoseismal IX.

map is highly sensitive to the expected intensity at a site and its attenuation with distance from the epicentre as also described in the previous section. This forms a major source of uncertainty in seismic hazard maps that in some cases overshadows all the other factors of uncertainty, even fault slip-rates, which govern the earthquake occurrence (Papanikolaou, 2011).

4.4.2. Quantitative-frequency of shaking seismic hazard maps

Fig. 10 shows how many times each locality receives enough energy to shake at intensity IX and higher over the past 15 ± 3 kyr assuming an homogeneous bedrock geology, a circular pattern of energy release and an 18 km radius of isoseismal IX. Highest hazard is observed, as expected, towards the hanging wall centre of the Sparta Fault (12 times in 15 ± 3 kyr) and diminishes towards the tips, following the slip-rate variability.

Fig. 11 shows the maximum expected intensities after considering the amplification due to the surface geology. Therefore, this map offers a locality specific shaking recurrence record rather than a fault specific record. The simple attenuation model decreases the intensity by: i) a single value, if two localities are equidistant from an epicentre, but one lies on Mesozoic or Tertiary limestone and the other lies on flysch/foredeep deposits and ii) two single values if two localities are within 18 km from the epicentre, but one lies on Mesozoic limestone and the other lies on Quaternary sediments. The town of Sparta lies closer to the hanging wall centre and is founded on Quaternary sediments, whereas surrounding villages are founded on alluvial fans and triangular facets which are regarded as highly vulnerable. Therefore, it will receive enough energy to shake at intensity X, 8 or 9 times (lies on the boundary) over 15 ± 3 kyr (therefore having a recurrence interval ranging from 1334 up to 2250 years). The latter implies that it experiences a destructive event similar to the 464 B.C. approximately every 1792 ± 458 years. As a result, the time independent and time dependent probabilities calculated for the town of Sparta are based on this locality specific

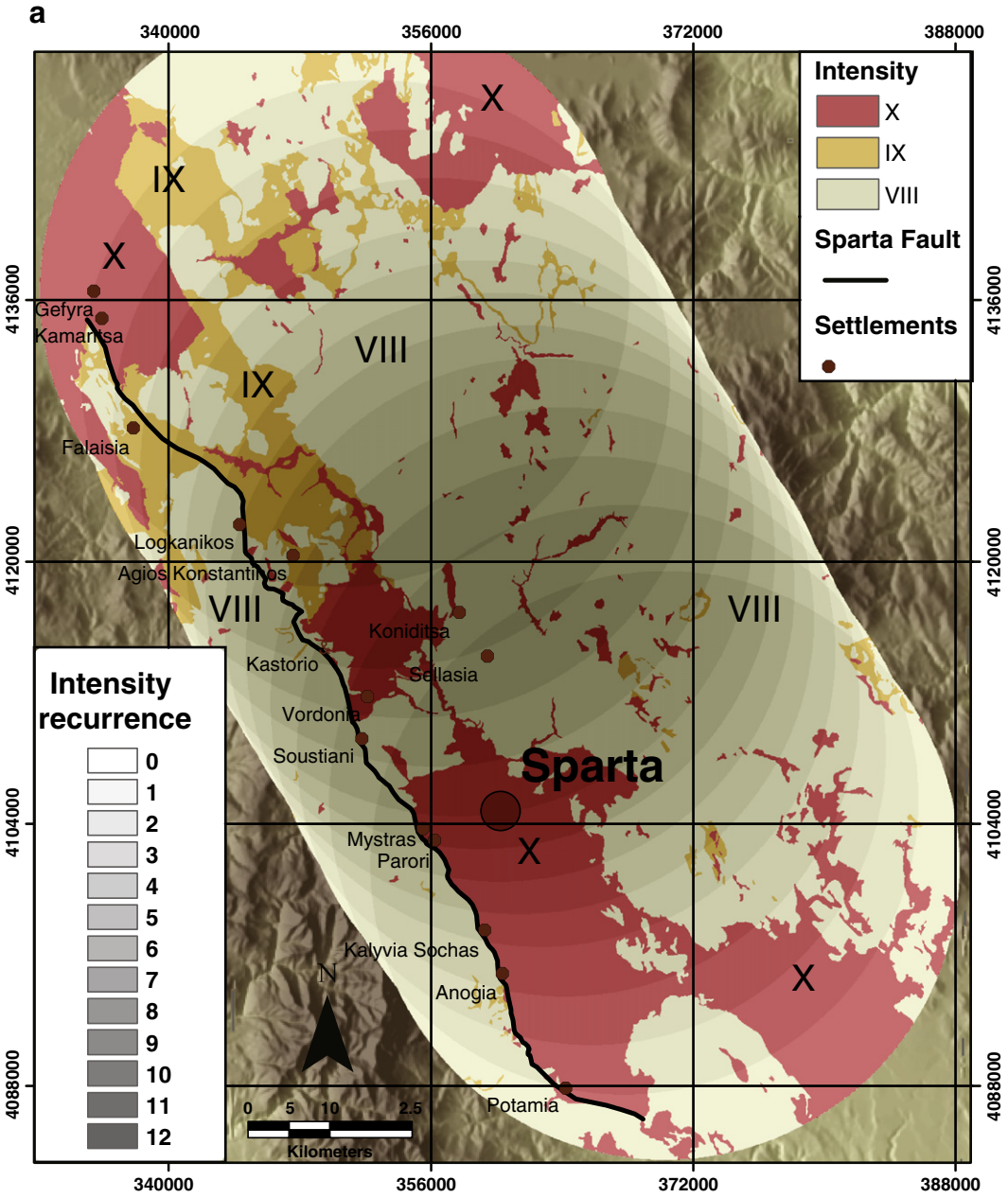

Fig. 11. Seismic hazard map for the Sparta Basin offering a locality specific shaking recurrence record rather than a fault specific record. It shows: a) the maximum expected intensities and their recurrence over the past 15 ± 3 kyr, after considering the bedrock geology.

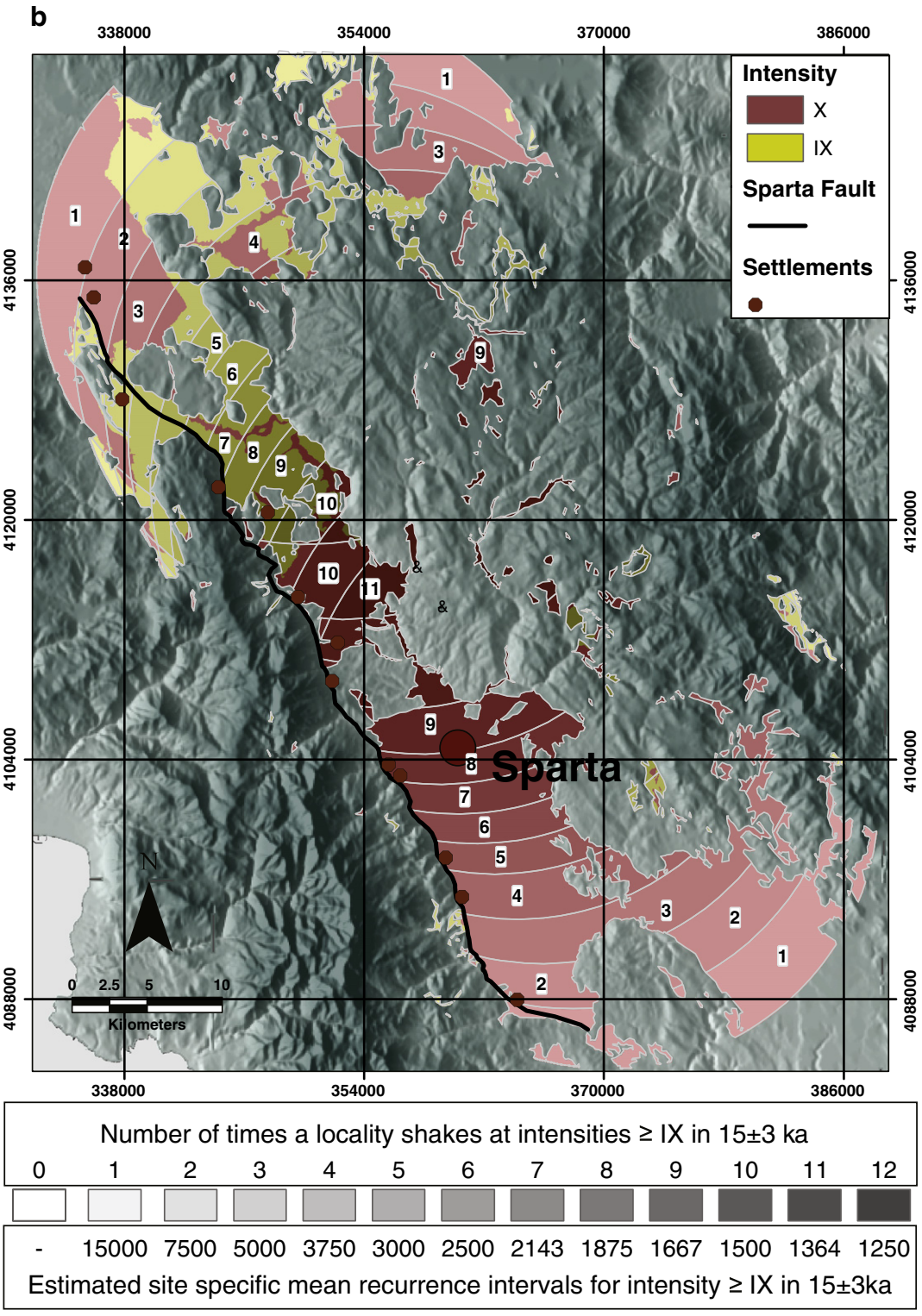

Fig. 11. Seismic hazard map for the Sparta Basin offering a locality specific shaking recurrence record rather than a fault specific record. It shows: b) the estimated site specific mean recurrence intervals for intensities ≥IX.

shaking recurrence, rather than the total fault specific recurrence, as is normally calculated in seismic hazard studies.

5. Time independent and time dependent probabilities for the town of Sparta

Average recurrence intervals are the main input data for the probabilistic seismic hazard analysis and should represent the long-term shaking record. The average recurrence intervals extracted from this study represent the long-term shaking record in a more complete way than the historical/instrumental catalogue since they incorporate several seismic cycles.

Probabilities can be extracted based on these average recurrence intervals, following the stationary Poisson model or a time dependent renewal statistical model. According to the Poisson model the probability of earthquakes is uniform in time. On the other hand, a time

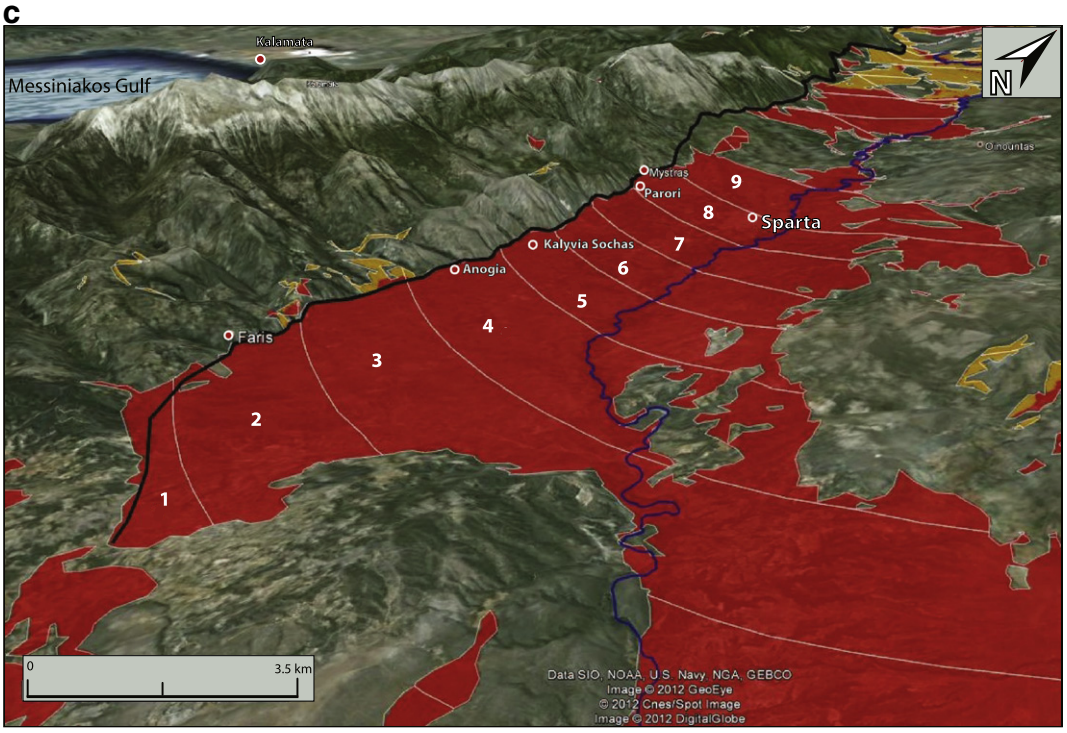

Fig. 11. Seismic hazard map for the Sparta Basin offering a locality specific shaking recurrence record rather than a fault specific record. It shows: c) 3D view of the southern part of the seismic hazard map, showing the number of times a locality receives enough energy to shake intensities ≥IX, in 15 ± 3 kyr.

dependent renewal model is based on the elastic rebound concept according to which the occurrence of a large earthquake releases the accumulated seismic energy and therefore decreases the probability for a near-future similar size event in the same region. However, as time since the last event increases, so does the probability.

5.1. Time independent probabilities

The simplest and most widely used probability model is the Poisson, which assumes that the probability does not vary in time and is thus fully determined by the long-term rate of occurrence of the rupture source (e.g. Reiter, 1990; Udias, 1999; WGCEP, 1999). The stationary Poisson model has no memory and it is the model of least information (Evison, 2001). If λ is the rate of occurrence of earthquakes of a given magnitude (M ~ 7.0) within a time t, the probability that n earthquakes take place within such interval is Poisson $= \frac{\lambda^n e^{-\lambda}}{n}$. If the occurrence of earthquakes follows a Poisson distribution, then the intervals of time t between consecutive earthquakes have an exponential distribution (Udias, 1999). In this case the equation for the probability density function is: $P(n) = \lambda e^{-\lambda \delta t}$, whereas the cumulative distribution function is $P = 1 - e^{-\lambda t}$ (Papoulis, 1991; Udias, 1999). This model is usually applied when no information other than the mean rate of earthquake production in known (WGCEP, 1999).

Overall, the best feature of the Poisson probability is that a forecast can be made without knowing when the last significant earthquake occurred, so according to this model odds do not change with time (Stein, 2003). Following the model of Poisson a time-independent probability of having shaking of intensity X is calculated for the town of Sparta of 0.56% for the next 10 years, 1.66% over the next 30 years and 2.75% over the next 50 years (Table 1).

However, the Poisson distribution has no memory and thus fails to incorporate the most basic physics of the earthquake cycle, according to which following a major earthquake another earthquake on the same fault segment is unlikely until sufficient time has elapsed for stress to gradually re-accumulate (e.g. Ellsworth et al., 1999; Ogata, 1999; WGCEP, 1999; Stein, 2002). The earthquake cycle is considered by the following time dependent renewal model.

5.2. Time dependent renewal model

The renewal model incorporates the concept of elastic rebound as described by Reid (1910). Large earthquakes are associated with a cycle of major stress drop and stress recovery, implying that recurrence intervals should follow a temporal pattern associated with a relatively narrow probability distribution (WGCEP, 1990). In a time dependent renewal model the occurrence probability of the next event only depends upon the time since the last event, the parameters of the renewal process, and of course the time interval of interest (WGCEP, 1999). Each renewal model is specified by a probability density function that defines the chance that failure will occur in the infinitesimal interval from t to t + Δt, where t is the time measured from the date of the last earthquake (WGCEP, 1999). Several statistical models have been proposed that are mathematical well-developed functions with well known statistical properties such as the Poisson, the Double exponential, Gaussian,

Table 1
Seismic hazard assessment for the town of Sparta. Time independent probabilities of having intensity X shaking at Sparta and input parameters for the time dependent probabilities (see Table 2).

Times shaken over 15 ± 3 kyr at intensity ≥X based on map of Fig. 11	T (in years) average recurrence interval	Date of the last event	Elapsed time (in years)	Poisson probabilities for the next 30 years (2012–2041)
8 or 9	1792 ± 458 yr	464 B.C.	2475	0.0166 or 1.66%

Weibull, Gamma, Brownian Passage time and lognormal (e.g. Ellsworth et al., 1999). However, with the exception of the Exponential model or Poisson process, which is rejected (e.g. Ellsworth et al., 1999; Ogata, 1999), all other models display generally similar probability density functions (Ellsworth et al., 1999). The choice of a probability density function can have an influence on the calculated value for a given fault, but unfortunately this decision is somewhat arbitrary because there is little quantitative basis for making it (Parsons, 2005). Despite the latter the lognormal and Brownian distributions are very similar and both are widely used (Parsons, 2005). A lognormal distribution has a long history since was initially proposed and applied by Nishenko and Buland (1987) and Nishenko and Singh (1987), confirmed by modelling (Brown et al., 1991) and also fitted the recurrence times of the repeating earthquakes near Parkfield (Nadeau et al., 1995). In this study the lognormal distribution has been used that is also favoured in extensional settings such as the Basin and Range (Chang and Smith, 2002).

Thus, a random variable x is lognormally distributed if its logarithm lnx is normally distributed. Since lnx is normally distributed, its mean, median, and mode are equal to T_m, but the mean, median and mode of x are distinct (Campbell, 1995). T_m and σ^2 denote the mean and variance of lnx, respectively. The two parameters are dimensionless since they relate to the logarithm; therefore the distribution of x is fully determined by these two parameters (Campbell, 1995). The lognormal distribution approaches the normal distribution as the variance approaches zero (Shimizu and Crow, 1988). Input parameters for the calculation of the probability are: i) T_e the elapsed time since the last event, ii) T_m the median recurrence interval; and iii) σ, a measure of the dispersion or spread in the recurrence time distribution (WGCEP, 1999). Time is set to zero at the occurrence of the most recent earthquake. The fraction of all earthquake recurrence times in an interval $(t, t+\Delta T)$ is obtained from the lognormal probability density function by integration (WGCEP, 1990):

$$P(t \le T \le t+\Delta T) = \int_{t}^{t+\Delta t} \frac{1}{u\sigma\sqrt{2\pi}} \exp\left\{\frac{-[\ln u/Tm]^2}{2\sigma^2}\right\} du.$$

σ is the uncertainty parameter and represents the standard deviation of the natural logarithm of the recurrence time. The uncertainty parameter σ is the square root of the sum of the squares of two components: a) the parametric uncertainty arising from uncertainties in the date of the last event and the slip-rate and b) the intrinsic uncertainty that reflects the event to event variability in recurrence time if T_m is perfectly known (Nishenko and Buland, 1987; WGCEP, 1990). The two sources of variability are independent, so the total variance is:

$$\sigma = \sqrt{\sigma_P^2 + \sigma_I^2}.$$

If the date of the previous earthquake is known the conditional probability that the earthquake will occur in the next interval $(T, T+\Delta T)$ can be determined, provided that it has not occurred prior to T_e (e.g. the time since the last earthquake) (Scholz, 2002).

Now the probability conditional on the earthquake not having occurred prior to T_e is (WGCEP, 1990):

$$P(T_e \le T \le T_e + \Delta T | T > T_e) = \frac{P(T_e \le T \le T_e + \Delta T)}{1 - P(0 \le T \le T_e)}.$$

The conditional probability is determined by dividing the area under the density function in the interval of interest by the area of the density function at times equal to or greater than the start of the interval of interest (WGCEP, 1999). Fig. 12 shows the lognormal probability density function and how conditional probabilities are calculated.

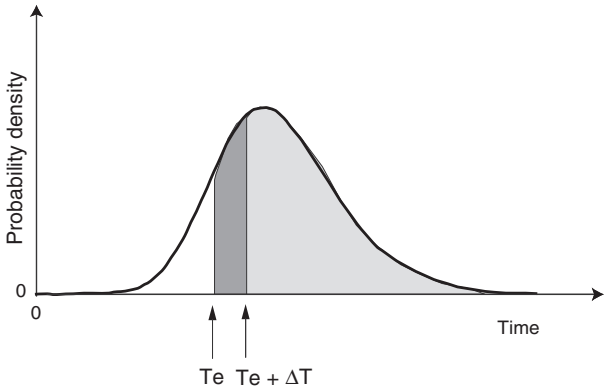

Fig. 12. Probability density function for earthquake recurrence. Conditional probability in interval $(T_e \le T \le T_e + T)$, given the elapsed time T_e since the last event, is the ratio of the area of dark shading to the sum of the areas with dark and light shading. After WGCEP (1990).

Probabilistic results depend strongly on the value of the uncertainty parameter σ. As σ increases the probability density broadens, its peak value decreases and is shifted away from T_m and closer to zero. Overall, with higher values of σ the probability density flattens and is insensitive to the precise value of T_m (Savage, 1992). The value of σ dictates the sensitivity of the forecast to the elapsed time so that as σ approaches to 1, becomes independent of the elapsed time (WGCEP, 1999). The latter implies that the value of sigma is critical for the calculated probabilities. The uncertainty parameter σ is the square root of the sum of the squares of the: a) parametric uncertainty and b) the intrinsic uncertainty. The town of Sparta experiences a strong event M~7.0 every 1792 ± 458 years, implying a parametric uncertainty of 0.255. Parametric uncertainty embodies only the uncertainty regarding the slip-rates, because the date since the last event (e.g. 464 B.C.) is accurately known based on the historical record. The intrinsic uncertainty that forms the major source of uncertainty reflects the natural event to event variability in recurrence. The intrinsic variation in the length of recurrence intervals from cycle to cycle, reflects the complexities in the accumulation and release of strain (Nishenko and Buland, 1987). According to Nishenko and Buland (1987) the standard deviation of recurrence intervals is a fixed fraction of the average recurrence interval, implying a relatively uniform, well behaved scale independent physical structure underlying the characteristic earthquake cycle. The value of the intrinsic variability of the recurrence intervals is one of the major unknowns and possibly different of each fault. There are several values reported worldwide ranging from 0.21 to 0.36 (Nishenko and Buland, 1987; McCalpin and Slemmons, 1998), implying a highly periodic behaviour up to 0.75 (Toda et al., 1998) which is closer to time-independent.

As far as the Sparta Fault is concerned, the cosmogenic isotope dating allows the recognition of several surface faulting events on the fault and offers a unique opportunity to extract its recurrence history. Indeed, the cosmogenic isotope dating provides a valuable record of the last 6 events that occurred before 12,900, 8400, 5900, 4500, 4000 and 2800 years ago (Benedetti et al., 2002). As a result, the recurrence intervals are 4500, 2500, 1400, 500 and 1200 years, respectively, exhibiting a poor periodic behaviour, with periods of clusters followed by periods of anticlustering. This implies an intrinsic variability of 0.77 which lies towards the extreme upper end of the values used worldwide (e.g. 0.75 from Toda et al., 1998). For such high intrinsic variability value, the total uncertainty σ is practically insensitive to the parametric uncertainty. Therefore, for the calculation of the conditional probabilities we used a σ value (aperiodicity) which is equal to the standard deviation divided by the mean recurrence time (or COV — coefficient of variation) of 0.77. Moreover, the

COV of 0.77 that has been extracted, most probably overestimates the intrinsic variability of recurrence through time, because it still contains both measurement error and intrinsic variability (e.g. McCalpin, 2009) and therefore we support that it represents the total uncertainty.

However, the recurrence intervals extracted from both cosmogenic localities do not represent the series of all characteristic earthquakes on the Sparta Fault, but a subset of them. This is because events occurring towards the northern part of the fault may have not been traced in both cosmogenic site sampling localities located southwards (see Figs. 10 and 11a), if surface ruptures did not reach the sites or were of low displacement (less than 20 cm). The latter is also highlighted if we consider that cosmogenic isotope dating showed that the two events recorded in Parori were not recorded in Anogia and vice versa, even though both localities are only 10 km apart. Moreover, Benedetti et al. (2002) did not sample the 2–3 m upper part of the free face in Parori, whereas in Anogia they report some smaller approximately 2–3 m high possible scarps in the immediate hanging wall. Missing events could severely modify the COV value. Indeed, McCalpin and Slemmons (1998) support that as the paleoearthquake chronologies get longer and contain more successive recurrence intervals, the spread of COVs among them decreases steadily. The longer a time window the more representative it will be of the complete fault history, which is expected to have a COV between 0.3 and 0.4. The latter may explain why the COV in Sparta displays such a high value. Overall, COV tends to be higher when the strain is partitioned on more than one fault, thus in areas where the fault pattern is complex and the deformation distributed (Sykes and Menke, 2006; Cowie et al., 2012). Specifically, lower values of COV are expected where the deformation is more localised and the long-term fault slip rate is higher (Cowie et al., 2012). In our study area, strain is localised on the Sparta Fault (see also Discussion), implying also a lower COV value. Following the above concerns, two additional lower COV values have been used, a 0.5 and a 0.36 (Table 2).

As discussed previously the coefficient of variation of the inter-event times is a major source of uncertainty and its exact value is unknown. Nishenko and Buland (1987) examined 53 recurrence intervals of characteristic events from segments of Circum-Pacific plate boundaries with histories of two or more recurrences, supporting a sigma value of 0.21. However, this value has been questioned by other workers (e.g., Savage, 1992; Toda et al., 1998). Goes (1996) analysed 52 recurrence series and concluded that the COV of recurrence (aperiodicity) was greater than 0.4. Ellsworth et al. (1999) analysed 37 worldwide series of recurrent earthquakes with at least four closed intervals (5 events) on the same fault segments and calculated a significantly higher value of 0.5 for the coefficient of variation compared to the value of 0.21 obtained from Nishenko and Buland (1987). In particular, Ellsworth et al. (1999) calculated a value of 0.58 for the aperiodicity of the Irpinia normal fault in the Southern Apennines based on paleoseimic data from Pantosti et al. (1993) and constitutes one of the few normal faults in his catalogue and the only one from the Mediterranean. On the other hand, Sykes and Menke (2006) after analysing several time intervals between large earthquakes for several fault segments along plate boundaries in Japan, Alaska, California, Cascadia, and Turkey concluded that the COV (aperiodicity) of 0.5 that is widely used in hazard analysis in the USA is an overestimate, and that faults are more regular in recurrence, supporting lower COV values similar to the McCalpin and Slemmons (1998) who promote a value of 0.36. Studies more recent than Nishenko and Buland (1987), even though they acknowledge that the σ value is highly unknown, tend to use higher values ranging from 0.28 to 0.75 (McCalpin and Nishenko, 1996; Toda et al., 1998; Ellsworth et al., 1999; WGCEP, 1999; Cramer et al., 2000; Parsons, 2005) so that the uncertainty on repeat times is not underestimated. Finally, recently Cowie et al. (2012) introduce a new measure, the slip-rate variability (SRV) and suggest that both the SRV and COV (coefficient of variation) are required to fully characterise the variability in fault behaviour.

Table 2
Conditional probabilities for the town of Sparta calculated for the year 2012 and the next 10, 30 and 50 years for different values of sigma.

σ	2012–2021 (10 years)	2012–2041 (30 years)	2012–2061 (50 years)
0.77	0.57%	1.69%	2.80%
0.50	1.00%	2.99%	4.93%
0.36	1.61%	4.76%	7.82%

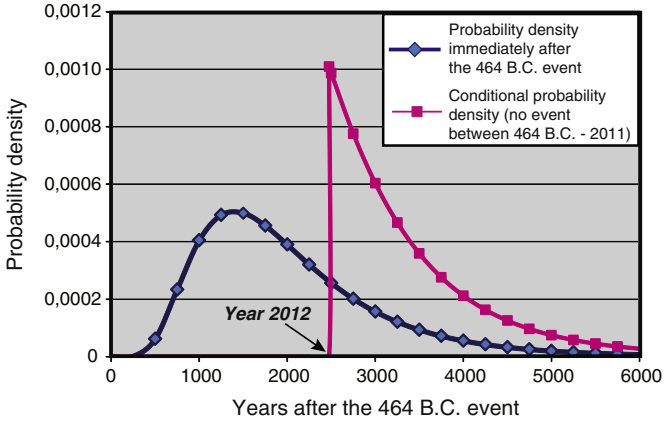

Fig. 13. Diagram showing the probability density for the town of Sparta immediately after the 464 B.C. event and the conditional probability density of future shaking of intensity ≥IX, considering that no event occurred since 2011. A sigma value of 0.5 is used.

Fig. 13 shows the probability density immediately after the 464 B.C. event as well as the conditional probability density, knowing that no event took place over the past 2475 years (up to the year 2011). The time-dependent probability for the next major event in the town of Sparta is 3.0% for the next 30 years and 4.9% over the next 50 years based on a COV = 0.5 that is preferred. Table 2 calculates the conditional probabilities for the year 2012 and the next 10, 30 and 50 years.

Following Table 2 and Fig. 14, by decreasing the sigma value from 0.77 to 0.5 and 0.36 the time-dependent probability for the next major event in the town of Sparta is increased from 1.7% to 3.0% and 4.8% for the next 30 years and from 2.8% to 4.9% and 7.8% over the next 50 years, respectively. This occurs because for smaller values

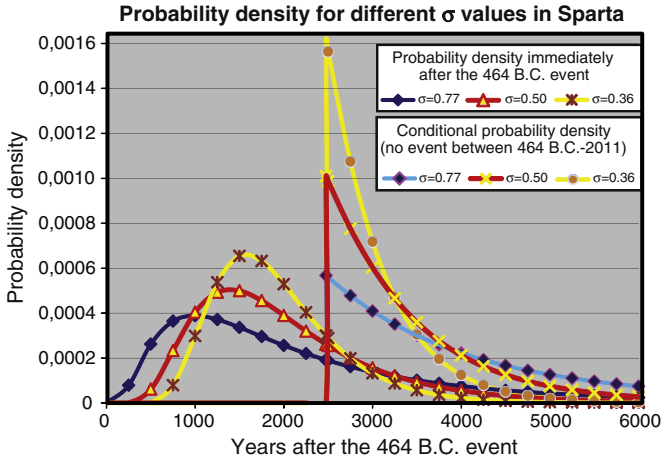

Fig. 14. Diagram showing the probability density and the conditional probability density for σ = 0.77, σ = 0.50 and σ = 0.36. When higher σ values are applied, uncertainties are increased, the probability distribution broadens, lowering the peak value and as a result the probabilities are less sensitive to the mean recurrence interval. This graph explains why higher conditional probabilities are calculated, when lower values of σ are introduced.

of σ, uncertainty regarding the irregularity of the inter-event times lessens and thus the probability density is strongly peaked and remains close to zero longer. The latter shows the significant influence that the sigma value exerts on the final results.

6. Discussion

The Sparta Fault system is a major structure that dominates the eastern flank of the Taygetos Mt and shapes the geological and geomorphological pattern of the region. The Evrotas river flows parallel to the Sparta Fault towards its hanging wall. Overall, fault slip-rates exceed sedimentation rates all along the basin. Therefore, the generation of extra volume due to successive large earthquakes is significantly higher compared to the sediment supply to the basin, implying that the Sparta–Evrotas basin is underfilled. This is also confirmed by several large alluvial fans that exist towards its fault trace. These fans are located between the present day sedimentation base of the basin and the fault trace where additional volume is created, forming a transfer zone or a bridge between the knick point and the base of sedimentation. The higher the discrepancy between basin widening–deepening rates and sediment supply rates, the higher the height of the alluvial fans. In addition, the occurrence of these alluvial fans in the immediate hanging wall of the fault prevents the Evrotas river from flowing towards the immediate hanging wall of the Sparta Fault, where the maximum subsidence is expected and divert it a few km eastwards towards the antithetic Sparta Fault. The antithetic Sparta Fault also produces subsidence, but has no such alluvial fans. Due to its short distance (~5 km) from the Sparta Fault, this antithetic structure most probably is linked at depth with the main Sparta Fault. The latter explains why this structure has not been treated as an independent structure and seismic source. The antithetic fault has a low slip-rate that is also confirmed by the long catchment profiles that cross this fault and exhibit no convexities as well as from the low k_{sn} values ($k_{sn}<30$).

Overall, long profile convexities can be revealed in all but one (Agios Konstantinos) rivers crossing the Sparta Fault. Moreover, the documented large scaled along-strike variations show that the central part of the Sparta Fault system appears to have undergone an increase in relative uplift rate compared to the north and southern part of the fault, indicating that the uplift rate diminishes as approaching the tips of the fault. Indeed, catchments are sensitive to along-stream variations in differential uplift as it is observed with changes in the profile concavity or steepness index along strike the fault system (Fig. 7). The latter is also confirmed by the calculated differences of k_{sn} between the outer ($k_{sn}<83$) and central parts ($121<k_{sn}<138$) of the Sparta Fault. Moreover, the height of the convex reaches in Soustianoi and Kastori channel profiles that outreaches 590 m, indicate that the Sparta Fault has been tectonically active as one hard-linked structure probably for the last few hundred thousand years. Prior to this linkage there were two separate segments with different lengths and displacements. This recent modification and linkage can potentially explain the absence of Upper Pleistocene sediments and alluvial fans and the smaller finite throw of the Vordonia–Kastori segment. In a few words, towards the central part of the Sparta Fault system, where no alluvial fan deposits and talus cones outcrop and the total throw is smaller, the Vordonia and Soustianoi catchment convex heights record the highest values as measured from the fault. This indicates that these high uplift rates recorded in the catchments are fairly young so that the geological pattern has not followed yet. This high uplift rate is probably the result due to the segment linkage so that the central part of the newly linked fault has to re-adjust to the new rates (e.g. Cowie, 1998; Gupta and Scholz, 2000; Cowie and Roberts, 2001). On the other hand, rivers crossing the antithetic structure, or localities where no significant active faults exist, appear to have typical concave up profile geometry. The above described exceptions of Koniditsa and Kolliniatiko catchments with small convexities along different lithological units help us set the criteria on discriminating whether these convexities are due to an increase of uplift rate or due to differential erosion in this area. It is clear that differential erosion in our study area can account up to 100 m, a value similar to Whittaker et al. (2008) for the similar setting of the southern Apennines. It is clear that the k_{sn} values correlate with the uplift rate of the fault, but no numerical relationship has been extracted. As a result, the ~0.8 mm/yr Sparta Fault exerts a significant impact on the k_{sn} values, whereas the antithetic lower slip-rate fault has no such influence. Therefore, one of the questions concerns the slip-rate threshold from which k_{sn} values are influenced. Considering the along strike slip-rate variations and the response of the convex reach, the threshold is estimated at approximately 0.4–0.5 mm/yr, but this needs further study. The geomorphological analysis demonstrated that the Sparta Fault behaves as one structure and that all segments have now been hard-linked. This is important for the seismic hazard analysis, since the fault is modelled as one seismic source.

Based on geodetic data, the central and southern Peloponnese shows little internal deformation (<2 mm/yr), suggesting that to first order this area is moving coherently with the wider Aegean (McClusky et al., 2000). GPS stations towards the eastern (LEON Station) and the western part (XRIS Station) of the Southern Peloponnese exhibit a 1.4 mm/yr velocity difference regarding the E–W direction. Within this area two major active fault systems are traced, the Sparta and the Kalamata Faults. This low geodetic deformation is also confirmed by recent data that shows an east–west arc-parallel extension in the southern Peloponnese with a velocity difference of 0.9 mm/yr from the Sparta GPS station to XRIS station and approximately 30 nstrain/yr on E–W extension has been calculated for the Sparta basin (Hollenstein et al., 2008). These values are in agreement with the ~0.8 mm/yr (12 m/15 kyr) post-glacial geological rates of the Sparta Fault and indicate that deformation is indeed localised.

Fig. 11 is a quantitative fault specific seismic hazard map based solely on geological data showing the maximum expected intensities after considering the amplification due to the surface geology. This map offers a locality specific shaking recurrence record rather than a fault specific record. This locality specific approach can be proved valuable in settings where more than one fault source exists so that each locality might experience damages from multiple faults (e.g. in Central Apennines several faults are closely spaced both along and across strike, see Roberts et al., 2004). The Sparta Fault is estimated to have generated 13 strong earthquakes in 15 ± 3 kyr that can produce intensities ≥IX. However, the town of Sparta which is the main population centre, due to its location in respect to the fault, should have experienced 8 or 9 times intensities ≥IX. The latter implies that the town of Sparta experiences a destructive event similar to the 464 B.C. approximately every 1792 ± 458 years from which time independent and time dependent probabilities have been extracted. These events dominate the seismic moment release. Considering that no other major earthquake has been generated by this fault since 464 B.C., so that the elapsed time (2475 years) exceeds the recurrence interval for the town of Sparta (1792 ± 458 years), then a future event could be imminent. The latter makes a time dependent assessment critical. Therefore, conditional probabilities were calculated based on a time dependent renewal model. As the elapsed time increases and more elastic strain is accumulated, so does the likelihood for the next earthquake. Time dependent conditional probabilities incorporate the elastic rebound concept and are preferred in localities where hazard is governed by one major structure such as the Sparta Fault.

Following the above, a considerably higher time-dependent probability ranging from 1.69% to 4.76% over the next 30 years is calculated for the town of Sparta compared to the time-independent probability of 1.66%. The time dependent clearly exhibits higher values because the elapsed time since the last event (2475 years) has exceeded the mean recurrence interval (1792 years). Therefore, the choice of probability model (Poisson or time dependent) has a significant effect on the results. Cornell and Winterstein (1988) showed that in practice, application of the Poison (exponential) model would be inappropriate

where the hazard is controlled by single features if the elapsed time exceeds the average recurrence time between such events.

Additionally, probabilistic results depend strongly on the value of intrinsic variability of recurrence intervals. The coefficient of variation of the distribution or the aperiodicity is a measure of the irregularity of the length of the intervals between successive events (Ellsworth et al., 1999). The poor periodic behaviour of the Sparta Fault, as extracted from the cosmogenic isotope studies, is represented by the very high value of COV (0.77). In this study, conditional probabilities were calculated based on: i) a 0.77 COV value which is extracted directly from the Sparta Fault rupturing record, but it is highly probable that is based on an incomplete series of earthquakes, ii) a lower conservative COV value of 0.5 which is widely used from most researchers worldwide (e.g. Ellsworth et al., 1999; Cramer et al., 2000; Chang and Smith, 2002; Parsons, 2005) and iii) a value of 0.36 which is regarded by several researchers as more representative (McCalpin and Slemmons, 1998; Sykes and Menke, 2006) particularly for localised structures such as the Sparta Fault. It is also common that different values for aperiodicity are used to tackle this problem (e.g. Chang and Smith, 2002). For example, the WGCEP (1999) used three different values for aperiodicity (0.3, 0.5 and 0.7) which are similar to the values used in our case. Following Section 5.2, time dependent probability results based on a 0.5 COV value are preferred. This value is used if no adequate catalogue exists to estimate the coefficient of variation (e.g. Parsons et al., 2000). The 0.36 COV value is more unlikely despite the fact that the Sparta Fault is a localised structure due to the irregularity of earthquake time intervals based on the subset extracted from the cosmogenic sites.

Fig. 14 shows the probability density for the town of Sparta for these three different σ values. When higher σ values are applied, uncertainties are increased, the probability distribution broadens, lowering the peak value and as a result the probabilities are less sensitive to the Tm (e.g. Savage, 1992). The probabilities then become less time dependent, approaching the time independent Poisson values. This is evident also from Tables 1 and 2 whereas with higher sigma values conditional probabilities approach the Poisson probabilities.

This time-dependent pattern clearly shows one major weakness that current seismic hazard maps retain since they have no memory, disregarding the seismic cycle concept. Another weakness concerns the incompleteness of the historical record where current hazard maps are based on it. In the Sparta case study we are indeed lucky simply because the 464 B.C. earthquake occurred soon after the Greek historical record was established. It demonstrates once again that major events M~7.0 can have recurrence intervals that clearly exceed not only the completeness period of the historical catalogues (which is considered less than 500 years for M~7.0 in Greece, Papazachos et al., 2000), but even the length of the Greek historical catalogue, one of the longest worldwide. However, this was not the case with the damaging earthquake in Kozani–Grevena, Greece, 1995 (Ms = 6.6) (Chatzipetros et al., 1998; Ambraseys, 1999), that occurred in a region characterised as aseismic, according to the existing national hazard map (E.P.P.O., 1995), due to the absence of earthquakes in the historical record. This region following the earthquake was later re-assessed as an area of higher risk (E.P.P.O.-A.C.E.G., 2001). Even today half of the hanging wall area of the Sparta Fault that could experience intensities ≥IX belongs to zone I (lowest category of seismic risk 0.16 g) of the national seismic building code (EAK-2003).

Overall, these probability values that are extracted from this study, both time independent and particularly time dependent are considered fairly high. Nevertheless this judgement is also highly subjective and varies from country to country, from researcher to researcher and possibly also from what is at stake. However, in Japan, one of the countries with the highest seismicity rates worldwide, thus similar to Greece, active faults are considered as high risk, if they have probabilities of rupturing >3% over the next 30 years (HERP, 2005). The conditional probabilities for the town of Sparta equal this value for the same time period, if a σ = 0.5 is used. Finally, despite the probabilities calculated above, it is inevitable that a large earthquake will occur sooner or later in Sparta. Therefore, local communities and civil protection agencies should maintain high quality building standards and awareness and should consider some medium to long-term retrofit projects for major public buildings that are considered weak.

7. Conclusions

The Sparta Fault has been examined in terms of its geometry, segmentation, drainage pattern and post-glacial throw, emphasising also how these parameters vary along strike. The geomorphological analysis demonstrated that all segments have now been hard-linked over the past few hundred thousand years and that the Sparta Fault behaves as one structure. This is important for the seismic hazard analysis, since the fault is modelled as one seismic source. Qualitative analysis of long profile catchments shows a significant difference in longitudinal convexity and the height of the convex reaches between the central and both the south and north parts of the fault system, leading to the conclusion of varying uplift rate along strike. Catchments are sensitive to along-stream variations in differential uplift as it is observed by the calculated differences of the steepness index k_{sn} between the outer (k_{sn}<83) and central parts (121<k_{sn}<138) of the Sparta Fault along strike the fault system.

By combining the long-term earthquake recurrence record with the historical record and the paleoseismological data, derived from fault scarp analyses, a high spatial resolution seismic hazard map has been constructed for the region of Sparta, predicting how many times each location should have been shaken by intensity ≥IX or higher over the past 15 ± 3 kyr considering also the bedrock geology. This map can be easily transformed into a map of recurrence intervals and following several assumptions, time-independent and time-dependent probabilities have been extracted. Time dependent probabilities are important because they incorporate the most basic physics of the earthquake cycle. A time-independent probability of 1.66% over the next 30 years and 2.75% over the next 50 years is calculated for the town of Sparta. A considerably higher time-dependent probability ranging from 1.69% to 4.76% over the next 30 years and from 2.80% to 7.82% over the next 50 years has been calculated (values of 2.99% and 4.93%, respectively based on a COV = 0.5, are preferred). The time dependent probability follows the seismic cycle concept and exhibits higher values because the elapsed time since the last event (2475 years) has exceeded the mean recurrence interval (1792 years). Finally, despite these relatively high calculated probabilities, half of the hanging wall area of the Sparta Fault that could experience intensities ≥IX, belongs to the lowest category of seismic risk (0.16 g) of the national seismic building code, underestimating the hazard. Therefore, a reassessment of the national seismic building code should be considered.

Acknowledgements

The Institution of State Scholarships of Greece (IKY) and the Antonios Papadakis scholarship from the National and Kapodistrian University of Athens are thanked for support. Reviews from both referees and the guest editor strongly improved the paper.

References

Allen, J.R.M., Brandt, U., Brauer, A., Hubberten, H.W., Huntley, B., Keller, J., Kraml, M., Mackensen, A., Mingram, J., Negendank, J.F.W., Nowaczyk, N.R., Oberhansli, H., Watts, W.A., Wulf, S., Zolitschka, B., 1999. Rapid environmental changes in southern Europe during the last glacial period. Nature 400, 740–743.

Ambraseys, N., 1999. Early earthquakes in the Kozani Area, Northern Greece. Tectonophysics 308, 291–298.

Armijo, R., Lyon-Caen, H., Papanastassiou, D., 1991. A possible normal fault rupture for the 464 B.C. Sparta earthquake. Nature 351, 137–139.

Benedetti, L., Finkel, R., Papanastasiou, D., King, G., Armijo, R., Ryerson, F., Farber, D., Flerit, F., 2002. Post-glacial slip history of the Sparta fault (Greece) determined by ^{36}Cl cosmogenic dating: evidence for non-periodic earthquakes. Geophysical Research Letters 29. http://dx.doi.org/10.1029/2001GL014510.

Bolt, B.A., 1999. Earthquakes. W.H. Freeman and Company, New York . 366 pp.
Boulton, S.J., Whittaker, A.C., 2009. Quantifying the slip rates, spatial distribution and evolution of active normal faults from geomorphic analysis: field examples from an oblique-extensional graben, southern Turkey. Geomorphology 104, 299–316.
Brown, S.R., Scholz, C.H., Rundle, J.B., 1991. A simplified spring-block model of earthquakes. Geophysical Research Letters 18, 215–218.
Campbell, J.W., 1995. The lognormal distribution as a model for bio-optical variability in the sea. Journal of Geophysical Research 100, 13,237–13,254.
Caputo, R., Monaco, C., Tortorici, L., 2006. Multiseismic cycle deformation rates from Holocene normal fault scarps on Crete (Greece). Terra Nova 18, 181–190.
Chang, W.-L., Smith, R.B., 2002. Integrated seismic hazard analysis of the Wasatch front, Utah. Bulletin of the Seismological Society of America 92, 1904–1922.
Chatzipetros, A.A., Pavlides, S.B., Mountrakis, D.M., 1998. Understanding the 13 May 1995 western Macedonia earthquake: a paleoseismological approach (1998). Journal of Geodynamics 26, 321–339.
Cornell, C.A., Winterstein, S.R., 1988. Temporal and magnitude dependence in earthquake recurrence models. Bulletin of the Seismological Society of America 78, 1522–1537.
Cowie, P.A., 1998. A healing-reloading feedback control on the growth rate of seismogenic faults. Journal of Structural Geology 20, 1075–1087.
Cowie, P.A., Roberts, G.P., 2001. Constraining slip rates and spacings for active normal faults. Journal of Structural Geology 23, 1901–1915.
Cowie, P.A., Shipton, Z.K., 1998. Fault tip displacement gradients and process zone dimensions. Journal of Structural Geology 20, 983–997.
Cowie, P.A., Whittaker, A.C., Attal, M., Roberts, G., Tucker, G.E., Ganas, A., 2008. New constraints on sediment-flux-dependent river incision: implications for extracting tectonic signals from river profiles. Geology 36, 535–538. http://dx.doi.org/10.1130/G24681A.1.
Cowie, P.A., Roberts, G.P., Bull, J.M., Visini, F., 2012. Relationships between fault geometry, slip rate variability and earthquake recurrence in extensional settings. Geophysical Journal International 189, 143–160.
Cramer, C.H., Petersen, M.D., Cao, T., Toppozada, T.R., Reichle, M., 2000. A time-dependent probabilistic seismic-hazard model for California. Bulletin of the Seismological Society of America 90, 1–21.
Degg, M.R., 1992. The ROA Earthquake Hazard Atlas project: recent work from the Middle East. In: McCall, G.J.H., Laming, D.J.C., Scott, S.C. (Eds.), Geohazards: Natural and Manmade. Chapman and Hall, London, pp. 93–104.
Dimadis, E. and Taktikos, S. 1989. 1:50000 Geological Map "Gythion", IGME.
Duval, A., Kirby, E., Burbank, D., 2004. Tectonic and lithologic controls on bedrock channel profiles and processes in coastal California. Journal of Geophysical Research 109 (F03002), 1–18.
E.P.P.O., 1995. New Greek Seismic Design Code. Earthquake Planning and Protection Organization, Ministry of Environment and Public Works, Athens . 138 pp.
E.P.P.O.-A.C.E.G., 2001. Greek Seismic Design Code 2000. Earthquake Planning and Protection organization, Association of Civil Engineers in Greece, Government Gazette 2184B/20-12-99 . 257 pp., Athens.
Eliet, P.P., Gawthorpe, R.L., 1995. Drainage development and sediment supply within rifts, examples from Sperchios basin mainland Greece. Journal of the Geological Society of London 152, 883–893.
Ellsworth, W.L., Matthews, M.V., Nadeau, R.M., Nishenko, S.P., Reasenberge, P.A., Simpson, R.W., 1999. A physically-based earthquake recurrence model for estimation of long-term earthquake probabilities. U.S. Geological Survey Open File Report 99-552. 23p.
Evernden, J.F., Thomson, J.M., 1985. Predicting seismic intensities. In: Ziony, J.I. (Ed.), Evaluating Earthquake Hazards in the Los Angeles Region — An Earth Science Perspective: U.S. Geological Survey Professional Paper, 1360, pp. 151–202.
Evison, F.F., 2001. Long-range synoptic earthquake forecasting: an aim for the millennium. Tectonophysics 338, 207–215.
Galanopoulos, A., 1961. A Catalogue of Shocks with Io ≥VII for the Years Prior to 1800. National Observatory of Athens,Seismological Institute.
Ganas, A., Papoulia, I., 2000. High-resolution, digital mapping of the seismic hazard within the Gulf of Evia Rift, Central Greece using normal fault segments as line sources. Natural Hazards 22, 203–223.
Gawthorpe, R., Hurst, J., 1993. Transfer zones in extensional basins: their structural style and influence on drainage development and stratigraphy. Journal of the Geological Society of London 150, 1137–1152.
Giraudi, C., 1995. Considerations on the significance of some post-glacial fault scarps in the Abruzzo Apennines (Central Italy). Quaternary International 25, 33–45.
Giraudi, C., Frezzotti, M., 1997. Late Pleistocene glacial events in the central Apennines, Italy. Quaternary Research 48, 280–290.
Goes, S.D.B., 1996. Irregular recurrence of large earthquakes: an analysis of historic and paleoseismic catalogs. Journal of Geophysical Research 101, 5739–5749.
Grandori, G., Drei, A., Perotti, F., Tagliani, A., 1991. Macroseismic intensity versus epicentral distance: the case of Central Italy. Tectonophysics 193, 165–171.
Gupta, A., Scholz, C.H., 2000. A model of normal fault interaction based on observations and theory. Journal of Structural Geology 22, 865–879.
HERP, 2005. National Seismic Hazard Maps for Japan (2005). Headquarter for Earthquake Research Promotion. http://www.jishin.go.jp/main/indexe.html.
Hollenstein, Ch., Müller, M.D., Geiger, A., Kahle, H.-G., 2008. Crustal motion and deformation in Greece from a decade of GPS measurements, 1993–2003. Tectonophysics 449, 17–40.
Hughes, P.D., Woodward, J.C., Gibbard, P.L., 2006. Quaternary glacial history of the Mediterranean mountains. Progress in Physical Geography 30, 334–364.
Jackson, J.A., White, N.J., 1989. Normal faulting in the upper continental crust: observations from regions of active extension. Journal of Structural Geology 11, 15–36.
Kirby, E., Whipple, K.X., 2001. Quantifying differential rock-uplift rates via stream profile analysis. Geology 108, 415–418.
Kirby, E., Whipple, K.X., 2003. Distribution of active rock uplift along the eastern margin of the Tibetan Plateau: inferences from bedrock channel longitudinal profiles. Journal of Geophysical Research 108 (B4/2217), 1–24.
Lee, K., Kim, J.-K., 2002. Intensity attenuation in the Sino-Korean craton. Bulletin of the Seismological Society of America 92, 783–793.
Lyon-Caen, H., Armijo, R., Drakopoulos, J., Baskoutas, J., Delibasis, N., Gaulon, R., Kouskouna, V., Latoussakis, J., Makropoulos, K., Papadimitriou, P., Papanastassiou, D., Pedotti, G., 1988. The 1986 Kalamata (South Peloponnesus) Earthquake: detailed study of a normal fault, evidences for east–west extension in the Hellenic arc. Journal of Geophysical Research 93, 14,967–15,000.
Mariolakos, I., Papanikolaou, D., 1981. The Neogene basins of the Aegean Arc from the paleogeographic and the geodynamic point of view. Int. Symp. On the Hellenic Arc and Trench (H.E.A.T.), Athens 1981, Proceedings, I, pp. 383–399.
Mariolakos, I., Fountoulis, I., Logos, E., Lozios, S., 1989. Surface faulting caused by the Kalamata (Greece) earthquakes (13.9.86). Tectonophysics 163, 197–203.
Mastronuzzi, G., Sanso, P., Stamatopoulos, L., 1994. The glacial landforms of the Peloponnisos (Greece). Rivista Geografica Italiana 101, 77–86.
McCalpin, J., 2009. Paleoseismology, 2nd edition. International Geophysics. 0074-6142, vol. 95. Elsevier Inc. http://dx.doi.org/10.1016/S0074-6142(09)95009-4.
McCalpin, J.P., Nishenko, S.P., 1996. Holocene paleoseismicity, temporal clustering and probabilities of future large (M>7) earthquakes on the Wasatch fault zone, Utah. Journal of Geophysical Research 101, 6233–6253.
McCalpin, J.P. and Slemmons, D.B. (1998). Statistics of paleoseismic data: Final Tech. Rept., Contr. 1434-HQ-96-GR-02752, GEO-HAZ Consulting, Estes Park, CO to U.S. Geol. Surv., Reston, VA, 62 p.
McClusky, S., Balassanian, S., Barka, A., Demir, C., Ergintav, S., Georgiev, I., Gurkan, O., Hamburger, M., Hurst, K., Kahle, H., Kastens, K., Kekelidze, G., King, R., Kotzev, V., Lenk, O., Mahmoud, S., Mishin, A., Nadariya, M., Ouzounis, A., Paradissis, D., Peter, Y., Prilepin, M., Reilinger, R., Sanli, I., Seeger, H., Tealeb, A., Toksoz, M.N., Veis, G., 2000. Global Positioning System constraints on plate kinematics and dynamics in the Eastern Mediterranean and Caucasus. Journal of Geophysical Research 105, 5695–5719.
Medvedev, S.V., 1965. Engineering Seismology. Israel Program for Scientific Translations, Jerusalem.
Michetti, A.M., Audemard, F.A., Marco, S., 2005. Future trends in paleoseismology: integrated study of the seismic landscape as a vital tool in seismic hazard analyses. Tectonophysics 408, 3–21.
Nadeau, R.M., Foxall, W., McEvilly, T.V., 1995. Clustering and periodic recurrence of microearthquakes on the San Andreas fault at Parkfield, California. Science 267, 503–507.
Nishenko, S.P., Buland, R., 1987. A generic recurrence interval distribution for earthquake forecasting. Bulletin of the Seismological Society of America 77, 1382–1399.
Nishenko, S.P., Singh, S.K., 1987. Conditional probabilities for the recurrence of large and great interplate earthquakes along the Mexican subduction zone. Bulletin of the Seismological Society of America 77, 2095–2114.
Ogata, Y., 1999. Estimating the hazard of rupture using uncertain occurrence times of paleoearthquakes. Journal of Geophysical Research 104, 17995–18014.
Pace, B., Peruzza, L., Visini, F., 2010. LASSCI2009.2: layered earthquake rupture forecast model for central Italy, submitted to the CSEP project. Annals of Geophysics 3, 85–97.
Pantosti, D., Schwartz, D.P., Valensise, G., 1993. Paleoseismology along the 1980 surface rupture of the Irpinia fault: implications for the Earthquake recurrence in the Southern Apennines, Italy. Journal of Geophysical Research 98, 6561–6577.
Papadopoulos, P., 1997. 1:50000 Geological Map "Megalopolis", IGME.
Papaioannou, Ch., 1984. Attenuation of seismic intensities and seismic hazard in the area of Greece. Ph.D. Thesis, University of Thessaloniki, 200pp.
Papanastassiou, D., 1999. Seismic hazard assessment in the area of Mystras–Sparta, south Peloponnesus, Greece, based on local seismotectonic, seismic, geologic information and on different models of rupture propagation. Natural Hazards 18, 237–251.
Papanastassiou, D., Gaki-Papanastasiou, K., Maroukian, H., 2005. Recognition of past earthquakes along the Sparta fault (Peloponnesus, southern Greece) during the Holocene, by combining results of different dating techniques. Journal of Geodynamics 40, 189–199.
Papanikolaou, D., Lykousis, V., Chronis, G., Pavlakis, P., 1988. A comparative study of neotectonic basins across the Hellenic arc: the Messiniakos, Argolikos, Saronikos and Southern Evoikos Gulfs. Basin Research 1, 167–176.
Papanikolaou, D., Royden, L., 2007. Disruption of the Hellenic arc: Late Miocene extensional detachment faults and steep Pliocene–Quaternary normal faults – or – what happened at Corinth? Tectonics 26 (TC5003). http://dx.doi.org/10.1029/2006TC002007.
Papanikolaou, I.D., 2003. Generation of high resolution seismic hazard maps through integration of earthquake geology, fault mechanics theory and GIS techniques in extensional tectonic settings. Unpublished Ph.D thesis, University of London, 437pp.
Papanikolaou, I.D., 2011. Uncertainty in intensity assignment and attenuation relationships: how seismic hazard maps can benefit from the implementation of the Environmental Seismic Intensity scale (ESI 2007). Quaternary International 242, 42–51.
Papanikolaou, I.D., Roberts, G.P., Michetti, A.M., 2005. Fault scarps and deformation rates in Lazio–Abruzzo, Central Italy: comparison between geological fault slip-rate and GPS data. Tectonophysics 408, 147–176.
Papanikolaou, I.D., Papanikolaou, D.I., 2007. Seismic hazard scenarios from the longest geologically constrained active fault of the Aegean. Quaternary International 171–172, 31–44.
Papanikolaou, I.D., Roberts, G.P., 2007. Geometry, kinematics and deformation rates along the active normal fault system in the Southern Apennines: implications for fault growth. Journal of Structural Geology 29, 166–188.
Papazachos, B.C., Papaioannou, C.P., 1997. The macroseismic field of the Balkan area. Journal of Seismology 1, 181–201.

Papazachos, B.C., Papazachou, C., 1997. The Earthquakes of Greece. Ziti Publications, Thessaloniki.
Papazachos, B.C., Comninakis, P.E., Karakaisis, G.F., Karakostas, B.G., Papaioannou, C.A., Papazachos, C.B., Scordilis, E.M., 2000. A catalogue of earthquakes in Greece and surrounding area for the period 550BC–1999. Publ. Geoph. Lab. University of Thessaloniki.
Papoulia, J., Stavrakakis, G., Papanikolaou, D., 2001. Bayesian estimation of strong earthquakes in the Inner Messiniakos fault zone, southern Greece, based on seismological and geological data. Journal of Seismology 5, 233–242.
Papoulis, A., 1991. Probability, random variables, and stochastic processes. McGraw-Hill Series . 576p.
Park, S., Elrick, S., 1998. Predictions of shear wave velocities in southern California using surface geology. Bulletin of the Seismological Society of America 88, 677–685.
Parsons, T., 2005. Significance of stress transfer in time-dependent earthquake probability calculations. Journal of Geophysical Research 110 (B05S02). http://dx.doi.org/10.1029/2004JB003190.
Parsons, T., Toda, S., Stein, R.S., Barka, A., Dieterich, J.H., 2000. Heightened odds of large earthquakes near Istanbul: an interaction-based probability calculation. Science 288, 661–665.
Pavlides, S., Caputo, R., 2004. Magnitude versus faults' surface parameters: quantitative relationships from the Aegean Region. Tectonophysics 380, 159–188.
Petersen, M.D., Bryant, W.A., Cramer, C.H., Reuchle, M.S., Real, C.R., 1997. Seismic ground-motion hazard mapping incorporating site effects for Los Angeles, Orange, and Ventura Counties, California: a geographic information system application. Bulletin of the Seismological Society of America 87, 249–255.
Pope, R.J., Wilkinson, K.N., Millington, A.C., 2003. Human and climatic impact on Late Quaternary deposition in the Sparta Basin piedmont: evidence from alluvial fan systems. Geoarcheology: An International Journal 18, 685–724.
Psonis, K., 1986. 1:50000 Geological Map “Kalamata”, IGME.
Psonis, K., 1990. 1:50000 Geological Map “Sparti”, IGME.
Psonis, K. and Latsoudas, C., 1983. 1:50000 Geological Map “Xirokampion”, IGME.
Reid, H.F., 1910. The mechanics of the earthquake. The California Earthquake of April 18, 1906. : Report of the State Earthquake Investigation Commission, 2. Carnegie Institute, Washington D.C. Publication no. 87, 192 pp.
Reiter, L., 1990. Earthquake Hazard Analysis. Columbia University Press, New York . 254 pp.
Roberts, G.P., 1996. Variation in fault-slip directions along active and segmented normal fault systems. Journal of Structural Geology 18, 835–845.
Roberts, G.P., Ganas, A., 2000. Fault-slip directions in central-southern Greece measured from striated and corrugated fault planes: comparison with focal mechanism and geodetic data. Journal of Geophysical Research 105, 23,443–23,462.
Roberts, G.P., Cowie, P., Papanikolaou, I., Michetti, A.M., 2004. Fault scaling relationships, deformation rates and seismic hazards: an example from the Lazio-Abruzzo Apennines, central Italy. Journal of Structural Geology 26, 377–398.
Savage, J.C., 1992. The uncertainty in earthquake conditional probabilities. Geophysical Research Letters 19, 709–712.
Scholz, C.H., 2002. The Mechanics of Earthquakes and Faulting. Cambridge University Press . 471 pp.
Shimizu, K., Crow, E.L., 1988. History, genesis and properties. In: Shimizu, K., Crow, E.L. (Eds.), The Lognormal Distribution: Theory and Applications. Marcel Dekker, New York, pp. 1–25.
Sibson, R.H., 1984. Roughness at the base of the seismogenic zone: contributing factors. Journal of Geophysical Research 89, 5791–5799.
Silva, G.P., Goy, J.L., Zazo, C., Bardajı, T., 2003. Fault-generated mountain fronts in southeast Spain: geomorphologic assessment of tectonic and seismic activity. Geomorphology 50, 203–225.
Stein, R.S., 2002. Parkfield's unfulfilled promise. Nature 419, 257–258.
Stein, R.S., 2003. Earthquake conversations. Scientific American 60–67.
Stewart, I.S., Hancock, P.L., 1994. Neotectonics. In: Hancock, P.L. (Ed.), Continental Deformation. Pergamon Press, pp. 370–409.
Sykes, L.R., Menke, W., 2006. Repeat times of large earthquakes: implications for earthquake mechanics and long-term prediction. Bulletin of the Seismological Society of America 95, 1569–1596.
Tataris, A., Marangoudakis, N., Katsikatsos, G., 1970. 1:50000 Geological Map “Astros”, IGME.
Theodoulidis, N.P., 1991. Contribution to the study of strong motion in Greece. Ph.D. Thesis, University of Thessaloniki, 500pp.
Toda, S., Stein, R.S., Reasenberg, P.A., Dieterich, H., Yoshida, A., 1998. Stress transferred by the 1995 Mw = 6.9 Kobe, Japan, shock: effect on aftershocks and future earthquake probabilities. Journal of Geophysical Research 103, 24,543–24,565.
Turowski, J.M., Lague, D., Hovius, N., 2009. Response of bedrock channel width to tectonic forcing: insights from a numerical model, theoretical considerations, and comparison with field data. Journal of Geophysical Research 114, F03016. http://dx.doi.org/10.1029/2008JF001133.
Udias, A., 1999. Principles of Seismology. Cambridge University Press. 475p.
Wells, D.L., Coppersmith, K.J., 1994. New empirical relationships among magnitude, rupture length, rupture width and surface displacement. Bulletin of the Seismological Society of America 84, 974–1002.
Whipple, K.X., Tucker, G.E., 2002. Implications of sediment-flux-dependent river incision models for landscape evolution. Journal of Geophysical Research 107, 1–20.
Whipple, K.X., Wobus, C., Crosby, B., Kirby, E., Sheehan, D., 2007. New Tools for Quantitative Geomorphology: Extraction and Interpretation of Stream Profiles from Digital Topographic Data. Geologic Society of America Annual Meeting, Boulder, CO.
Whittaker, A.C., Attal, M., Cowie, P.A., Tucker, G.E., Roberts, G., 2008. Decoding temporal and spatial patterns of fault uplift using transient river long profiles. Geomorphology 100, 506–526.
Wobus, C., Whipple, K., Kirby, E., Snyder, N., Johnson, J., Spyropoulou, K., Crosby, B., Sheehan, D., 2006. Tectonics from topography: procedures, promise, and pitfalls. Tectonics, Climate, and Landscape Evolution: Special Paper — Geological Society of America, 398, pp. 55–74.
Working Group on California Earthquake Probabilites (WGCEP), 1990. Probabilities of large earthquakes in the San Fransisco Bay region, California. U.S. Geological Survey Circular 1053 51 pp.
Working Group on California Earthquake Probabilities, (WGCEP), 1999. Preliminary report: earthquake probabilities in the San Francisco Bay region: 2000–2030 — a summary of findings. USGS Open-File Report 99–517.
Working Group on California Earthquake Probabilities, 2002. Earthquake probabilities in the San Francisco Bay region: 2002–2031. USGS Open-File Report 03-214.
Yeats, R.S., Prentice, C.S., 1996. Introduction to special section: paleoseismology. Journal of Geophysical Research 101, 5847–5853.
Zindros, G. and Exindavelonis, P., 2002. 1:50000 Geological Map “Kollinae”, IGME.